On the Effect of Surface Friction and Upward Radiation of Energy on Equatorial Waves

JONATHAN LIN[a] AND KERRY EMANUEL[a]

[a] *Lorenz Center, Department of Earth, Atmospheric, and Planetary Sciences, Massachusetts Institute of Technology, Cambridge, Massachusetts*

(Manuscript received 20 July 2021, in final form 2 December 2021)

ABSTRACT: In theoretical models of tropical dynamics, the effects of both surface friction and upward wave radiation through interaction with the stratosphere are oft-ignored, as they greatly complicate mathematical analysis. In this study, we relax the rigid-lid assumption and impose surface drag, which allows the barotropic mode to be excited in equatorial waves. In particular, a previously developed set of linear, strict quasi-equilibrium tropospheric equations is coupled with a dry, passive stratosphere, and surface drag is added to the troposphere momentum equations. Theoretical and numerical model analysis is performed on the model in the limits of an inviscid surface coupled to a stratosphere, as well as a frictional surface under a rigid lid. This study confirms and extends previous research that shows the presence of a stratosphere strongly shifts the growth rates of fast-propagating equatorial waves to larger scales, reddening the equatorial power spectrum. The growth rates of modes that are slowly propagating and highly interactive with cloud radiation are shown to be negligibly affected by the presence of a stratosphere. Surface friction in this model framework acts as purely a damping mechanism and couples the baroclinic mode to the barotropic mode, increasing the poleward extent of the equatorial waves. Numerical solutions of the coupled troposphere–stratosphere model with surface friction show that the stratosphere stratification controls the extent of tropospheric trapping of the barotropic mode, and thus the poleward extent of the wave. The superposition of phase-shifted barotropic and first baroclinic modes is also shown to lead to an eastward vertical tilt in the dynamical fields of Kelvin wave–like modes.

KEYWORDS: Atmosphere; Kelvin waves; Madden-Julian oscillation; Stratosphere-troposphere coupling; Friction; Tropical variability; Waves, atmospheric

1. Introduction

Reduced models of the tropical atmosphere have found much success in replicating many characteristics of the tropical circulation. Of prominence are theoretical models that reduce the linear, primitive equations to the shallow-water equations by use of only the first baroclinic mode (Matsuno 1966; Gill 1980). Indeed, remarkable evidence of the linear and neutral equatorial waves that arise from the Matsuno–Gill model have been documented in the tropics (Wheeler and Kiladis 1999). The first baroclinic mode has also been used extensively in simple models of the tropics, from studies of intraseasonal oscillations (Emanuel 1987; Sobel et al. 2001) to steady circulations (Neelin and Held 1987; Emanuel et al. 1994; Neelin and Zeng 2000; Sobel and Bretherton 2000), among many others.

While the first baroclinic mode is certainly a prominent feature of the tropical atmosphere (Xu and Emanuel 1989), observational data and analysis have suggested the existence of another vertical mode, the second (stratiform) baroclinic mode (Mapes and Houze 1995; Straub and Kiladis 2002). These observations have led to a plethora of theoretical studies that analyze how the interaction between the first and second baroclinic modes can lead to instability in equatorial waves (Mapes 2000; Kuang 2008b).

Perhaps curiously left behind is the barotropic mode, even though it does indeed survive the strict quasi-equilibrium assumption; in fact strict quasi-equilibrium eliminates all but the barotropic and first baroclinic modes (Emanuel 1987; Neelin and Zeng 2000). The barotropic mode can be excited in linear models of equatorial waves through coupling to the first baroclinic mode via surface friction (Wang 1988; Wang and Rui 1990; Moskowitz and Bretherton 2000) or removal of the rigid-lid assumption (Yano and Emanuel 1991). Note that nonlinearity can lead to excitement of the barotropic mode, even under a rigid lid and no surface friction (Neelin and Zeng 2000). In this study, we build on the linear, strict quasi-equilibrium model first formulated in Khairoutdinov and Emanuel (2018, hereafter KE18) and further analyzed in Emanuel (2020, hereafter E20), and investigate how excitation of the barotropic mode through both surface friction and coupling to the stratosphere affects the growth, structure, and propagation of equatorial waves.

Baked into the modal decomposition of many simple models of the tropics is the rigid-lid assumption, since it dramatically simplifies analytic solutions. However, in reality the tropopause does not act as a rigid lid on the troposphere. While it is true the stratosphere has a larger stratification than the troposphere, the stratification in the stratosphere is not infinite. A "leaky-lid" analogy is more accurate, as wave energy can radiate to the stratosphere.

Denotes content that is immediately available upon publication as open access.

Corresponding author: Jonathan Lin, Jonathan Lin, jzlin@mit.edu

DOI: 10.1175/JAS-D-21-0199.1

A few studies have investigated the impact of a stratification jump at the tropopause on the evolution of a wave in the atmosphere. Yano and Emanuel (1991) extends the tropical intraseasonal model introduced in Emanuel (1987) by imposing a dry, passive stratosphere above the troposphere, and found that adding a stratosphere strongly damps the smallest scale $v = 0$ waves, shifting the growth rates to the larger scales. Note that Yano and Emanuel (1991) did not look at higher-order equatorial waves, and only focused on $v = 0$ waves. By imposing wave-radiation boundary conditions, other studies have found similar effects: that the effect of the stratosphere is a dampening one (Moskowitz and Bretherton 2000; Kuang 2008a). Chumakova et al. (2013) further investigates the leaky-lid effect by deriving a set of vertical, dissipative modes using the 2D, linear, Boussinesq equations, overlaying a stratosphere with buoyancy frequency N_2 over a troposphere with buoyancy frequency N_1, where $N_2 > N_1$. In their model, a new barotropic-like mode appears with a fast damping time scale. However, the vertical modes of Chumakova et al. (2013) are not orthogonal; they have also been criticized as unphysical, since the energy is unbounded with height, and they also do not admit steady state solutions to steady state heating (Edman and Romps 2017). Regardless of the exact specifics in applying a leaky lid above a troposphere, the inclusion of a stratosphere tends to shift growth rates of unstable modes to larger scales and allows the barotropic mode to be excited.

There have also been many studies that have investigated the role surface friction plays in modifying equatorial waves, and more prominently, the Madden–Julian oscillation (MJO). These theories based on conditional instability of the second kind (CISK), in which surface friction was postulated to act, through its induced moisture convergence, as a destabilizing mechanism for convectively coupled equatorial waves (Wang 1988; Wang and Rui 1990; Moskowitz and Bretherton 2000). Wang (1988) and Wang and Rui (1990) formulated a 2.5-layer "frictional WAVE-CISK" model (two tropospheric layers and a thin frictional boundary layer) in which the barotropic mode can be excited through surface friction. The surface friction acts to induce vertical motion at the top of the boundary layer, which can amplify wave disturbances if correlated with temperature anomalies. CISK theories have received much criticism [see Emanuel et al. (1994) and Neelin and Yu (1994)], since they violate the convective statistical equilibrium hypothesis, where the rate of production of convectively available potential energy (CAPE) by the large-scale environment is very nearly balanced by its consumption via convection (Arakawa and Schubert 1974). In the context of surface friction, this means that surface convergence is a by-product and not a driver of convection. Indeed, observations in the tropics support the statistical equilibrium model for convection in the tropics (Betts 1982; Xu and Emanuel 1989). Further, numerical simulations of large-scale equatorial waves do not support the idea that surface friction acts as a destabilizing mechanism for large-scale equatorial waves (Chao and Chen 2001).

Surface friction and boundary layer convergence have also been cited as one mechanism for moistening of the lower troposphere by shallow upward motion east of the MJO center (Wang 1988; Hsu and Li 2012; Adames and Wallace 2014). In theoretical models, this mechanism has been shown to influence the propagation speed and growth rates of the MJO through modulation of the gross moist stability (Sobel and Maloney 2013; Adames and Kim 2016).

In this study, we will show how surface friction and interaction with the stratosphere through upward wave energy radiation modify the characteristics of equatorial waves. The rigid-lid assumption is removed by explicitly coupling a passive and dry stratosphere on top of a convecting troposphere, and the energy density of solutions is enforced to decay with height. Surface drag is imposed on a thin boundary layer at the surface. In particular, we will focus on how the two aforementioned mechanisms can excite the barotropic mode. More uniquely, the barotropic mode in this study does not separate convective heating from large-scale thermodynamics, and thus it does not violate the strict quasi-equilibrium hypothesis. The study will extend on the results of Yano and Emanuel (1991), which only investigated the impact of surface friction and the stratosphere on the growth rates of $v = 0$, WISHE-amplified equatorial waves.

The paper is organized as follows. Section 2 describes the linear model. Section 3 presents the solutions of the linear model. The paper concludes with a discussion and summary in section 4.

2. Linear model

In this section, we describe and formulate the governing equations of our linear model. The model formulation is separated into two parts: section 2a, which describes the tropospheric model, and section 2b, which describes the stratospheric model.

a. Strict quasi-equilibrium troposphere

KE18 and E20 derive and analyze an equation set for a linear system that describes the dynamics and thermodynamics of an atmosphere that maintains a vertically constant saturation moist entropy s^* in the free troposphere. However, in both of those studies, the authors assume a rigid lid and frictionless surface. Hence, in their model, only the baroclinic mode can be excited, and upward radiation into the stratosphere is absent.

Here we derive nearly equivalent dynamics, but remove the rigid-lid hypothesis and include the barotropic mode. To begin, we first apply a Galerkin decomposition of the vertical modes of the troposphere and truncate all modes except the first two basis functions, V_0 and V_1, which are defined as the barotropic and baroclinic modes, respectively (Neelin and Zeng 2000). Mathematically, they are as follows:

$$V_0 = 1, \tag{1}$$

$$V_1 = \frac{\overline{T}(p) - [\overline{T}]}{T_b - [\overline{T}]}, \tag{2}$$

where $\overline{T}$ is the basic state temperature, T_b is the boundary layer temperature, and $[\overline{T}]$ is the pressure-weighted vertical

average of temperature. The operator $[\cdot] = (1/\Delta p)\int_{p_t}^{p_s} \cdot\, dp$ is the pressure-weighted vertical average along a moist adiabat, where p_s is the surface pressure, p_t is the tropopause pressure, and $\Delta p = p_s - p_t$. As is standard for vertical modes, the basis functions are orthogonal, or $\int_{p_s}^{p_t} V_0 V_1\, dp = 0$. Furthermore, note that $[V_1] = 0$. From this vertical mode decomposition, we assume separable dependencies between the horizontal and vertical modes as follows:

$$\phi(x,y,p,t) = \phi_0(x,y,t) + \phi_1(x,y,t),$$

and likewise for the other prognostic variables.

For a strict quasi-equilibrium troposphere in which the saturation moist entropy s^* is constant with height, linearized geopotential perturbations are directly connected to s^* perturbations (Emanuel 1987):

$$\frac{\partial \phi'}{\partial p} = -\left(\frac{\partial T}{\partial p}\right)_{s^*} s^{*\prime}, \tag{3}$$

where prime superscripts indicate perturbation quantities. The above may be directly integrated from the surface upward to yield the following:

$$\phi'(p) = \phi_b' + s^{*\prime}(\overline{T}_b - \overline{T}(p)), \tag{4}$$

where ϕ_b' is the geopotential in the boundary layer. When non-dimensionalized (see appendix A for details), Eq. (4) yields

$$\phi'(p) = \phi_b' + (1 - V_1)s^{*\prime}. \tag{5}$$

Note, the geopotential can be separated into its barotropic and baroclinic components:

$$\phi_0(x,y,t) = (\phi_b' + s^{*\prime})V_0, \tag{6}$$

$$\phi_1(x,y,p,t) = -s^{*\prime}V_1. \tag{7}$$

The pressure-weighted vertical average operator is also applied to Eq. (4) to give

$$\phi_b' = [\phi]' + s^{*\prime}([\overline{T}] - \overline{T}_b), \tag{8}$$

which in non-dimensional form is

$$\phi_b' = \phi_0' - s^{*\prime}. \tag{9}$$

Unlike the purely baroclinic motions described in KE18, the geopotential now contains contributions from the barotropic mode. Note that Eq. (5) can be evaluated at the tropopause and combined with Eq. (9) to obtain the tropopause geopotential ϕ_{tp}', which will be required to couple the system to the stratosphere:

$$\phi_{\mathrm{tp}}' = \phi_0' - V_1(\hat{p}_t)s^{*\prime}, \tag{10}$$

where $\hat{p}_t$ is the non-dimensional tropopause pressure.

Next, we formulate the full equations of motion on an equatorial β plane, adding in surface friction, which is represented as applying drag on an infinitesimally small boundary layer:

$$\frac{D\mathbf{V}}{Dt} = -\nabla\phi - \mathbf{k} \times \beta y\mathbf{V} - \delta(p - p_s)\frac{C_d}{h_b}|\mathbf{V}|\mathbf{V}, \tag{11}$$

where $\mathbf{V}$ is the vector wind, β is the meridional gradient of the Coriolis force, δ is the Dirac delta function, p is pressure, C_d is the drag coefficient, and h_b is the boundary layer depth. Note the surface stress is parameterized using the bulk aerodynamic drag formula. Linearizing around surface easterlies, non-dimensionalizing according to details in appendix A, substituting in Eq. (5), and dropping all primes of perturbation quantities, we obtain the following:

$$\frac{\partial u}{\partial t} = -\frac{\partial \phi_b}{\partial x} + (1 - V_1)\frac{\partial s^*}{\partial x} + yv - 2Fu\delta(\hat{p} - \hat{p}_s), \tag{12}$$

$$\frac{1}{\delta_x}\frac{\partial v}{\partial t} = -\frac{\partial \phi_b}{\partial y} + (1 - V_1)\frac{\partial s^*}{\partial y} - yu - \frac{F}{\delta_x}v\delta(\hat{p} - \hat{p}_s), \tag{13}$$

where F is the non-dimensional surface friction coefficient and δ_x represents the magnitude of zonal geostrophy (corresponding to δ in KE18). Note that the factor of 2 appears in Eq. (12) from assuming mean easterly flow in the zonal direction; it is absent from Eq. (13) from the assumption of no mean meridional flow. Finally, we project the linearized horizontal momentum equations onto the barotropic and baroclinic modes:

$$\frac{\partial u_0}{\partial t} = -\frac{\partial \phi_0}{\partial x} + yv_0 - 2F(u_0 + u_1), \tag{14}$$

$$\frac{1}{\delta_x}\frac{\partial v_0}{\partial t} = -\frac{\partial \phi_0}{\partial y} - yu_0 - \frac{F}{\delta_x}(v_0 + v_1), \tag{15}$$

$$\frac{\partial u_1}{\partial t} = \frac{\partial s^*}{\partial x} + yv_1 - 2F(u_0 + u_1), \tag{16}$$

$$\frac{1}{\delta_x}\frac{\partial v_1}{\partial t} = \frac{\partial s^*}{\partial y} - yu_1 - \frac{F}{\delta_x}(v_0 + v_1). \tag{17}$$

Next, we enforce mass continuity through the continuity equation in pressure coordinates:

$$\frac{\partial u}{\partial x} + \frac{\partial v}{\partial y} + \frac{\partial \omega}{\partial p} = 0, \tag{18}$$

where ω is the pressure vertical velocity. Integrating the continuity equation from the surface to the tropopause, non-dimensionalizing, and using the fact that $[V_1] = 0$:

$$\int_{\hat{p}_s}^{\hat{p}_t} \nabla_H \cdot \mathbf{V}\, d\hat{p} = \frac{\partial u_0}{\partial x} + \frac{\partial v_0}{\partial y} = \omega(\hat{p}_t), \tag{19}$$

where we have used zero vertical velocity condition at the lower boundary, and $\omega(\hat{p}_t)$ is the non-dimensional tropopause vertical velocity. Equation (19) shows that the tropopause

vertical velocity is only a function of the divergence of the barotropic mode, as the baroclinic mode is zero at the tropopause, by definition.

Finally, the thermodynamic equations in the troposphere link the dynamics to the thermodynamics, and are only slightly modified from KE18 and E20 in that horizontal diffusion is removed and $\kappa = 1$:[1]

$$\frac{\partial s^*}{\partial t} = (1 + C)s_m - w - \alpha u_b - \chi s^*, \tag{20}$$

$$\gamma \frac{\partial s_m}{\partial t} = -Ds^* - \alpha u_b - Gw + Cs_m, \tag{21}$$

where s_m is a characteristic moist entropy of the free troposphere, $w = -\partial u_b/\partial x - \partial v_b/\partial y$ is a proxy for the midlevel vertical velocity based on the boundary layer zonal velocity, $u_b = u_0 + u_1$, and boundary layer meridional velocity $v_b = v_0 + v_1$. The non-dimensional coefficients C, α, χ, D, G, and γ are described and formulated in detail in KE18. Briefly, C represents the strength of cloud radiative feedback, α is the wind-induced surface heat exchange (WISHE) feedback parameter, χ is boundary layer damping, D is entropy damping, G is the gross moist stability, and γ modifies the time scale of tropospheric entropy. In this model, the effects of moisture are encapsulated into the vertically integrated moist entropy, which is assumed to change through surface enthalpy fluxes, cloud-radiative feedbacks, vertical advection, and entropy damping. Note that many of the thermodynamic variables are also non-dimensionalized by factors that include the bulk precipitation efficiency (Khairoutdinov and Emanuel 2018).

Equations (14)–(17) and (19)–(21) formulate the tropospheric system, where u_0, v_0, u_1, v_1, ϕ_0, s^*, and s_m are the unknown variables. Note that the linear system is not complete: additional specification of the vertical velocity at the tropopause is required to complete the system. As mentioned previously, studies that assume a rigid lid set the tropopause velocity to be zero. Other studies parameterize the tropopause dynamics using a wave-radiation upper boundary condition (Moskowitz and Bretherton 2000; Kuang 2008a). In this study, we take a different approach and couple the vertical velocity to an explicit stratosphere model, as will be derived in section 2b.

b. Coupling to the stratosphere

In this section, we couple a dry, passive stratosphere to the strict quasi-equilibrium troposphere described in section 2a. We choose to represent a dry and passive stratosphere using the linearized, inviscid primitive equations in log-pressure coordinates and in hydrostatic balance [see chapter 3 of Andrews et al. (1987)]:

$$\frac{\partial u_s'}{\partial t} = -\frac{\partial \phi_s'}{\partial x} + \beta y v_s', \tag{22}$$

$$\frac{\partial v_s'}{\partial t} = -\frac{\partial \phi_s'}{\partial y} - \beta y u_s', \tag{23}$$

$$\frac{\partial u_s'}{\partial x} + \frac{\partial v_s'}{\partial y} + \frac{1}{\rho_s}\frac{\partial\left(\rho_s w_s^{*\prime}\right)}{\partial z^*} = 0, \tag{24}$$

$$\frac{\partial}{\partial t}\frac{\partial \phi_s'}{\partial z^*} + w_s^{*\prime} N^2 = 0, \tag{25}$$

where subscript s denotes quantities in the stratosphere, w_s^* is the log-pressure vertical velocity, N^2 is the buoyancy frequency, ρ_s is the basic state density, and the log-pressure vertical coordinate $z^* \equiv -H\ln(p/p_t) + 1$ is defined such that $z^* = 1$ is the bottom boundary, or the tropopause. H is the dimensional tropopause height. Equations (22)–(25) are non-dimensionalized according to notation shown in appendix A, with the additional specification that the non-dimensional density decays exponentially with a scale height H_s. The resulting, non-dimensional equations are shown in Eqs. (26)–(30), with primes removed from perturbation quantities:

$$\frac{\partial u_s}{\partial t} = -\frac{\partial \phi_s}{\partial x} + y v_s, \tag{26}$$

$$\frac{1}{\delta_x}\frac{\partial v_s}{\partial t} = -\frac{\partial \phi_s}{\partial y} - y u_s, \tag{27}$$

$$\frac{\partial u_s}{\partial x} + \frac{\partial v_s}{\partial y} + \frac{1}{\rho_s}\frac{\partial\left(\rho_s w_s^*\right)}{\partial z^*} = 0, \tag{28}$$

$$\frac{\partial}{\partial t}\frac{\partial \phi_s}{\partial z^*} + w_s^* S = 0, \tag{29}$$

$$\rho_s = \exp\left[\frac{H}{H_s}(1 - z^*)\right], \tag{30}$$

where S is a non-dimensional stratospheric stratification. For Earth-like parameters, the non-dimensional stratification is in the range of $S \approx [25\text{–}150]$.

It is important to note that these equations form a complete system by themselves. The stratospheric linear system admits neutral equatorial wave solutions under a rigid-lid upper boundary condition. However, under a upward wave radiation boundary condition, all of the solutions decay exponentially in time since there is no forcing in the stratosphere model and wave energy escapes upward. Growing solutions that satisfy the upward wave radiation boundary condition in the stratosphere are possible, however, if there is mechanical forcing from the troposphere via the tropopause. To investigate these kinds of solutions, we must couple the troposphere system with the stratosphere system in a consistent fashion. Classical coupling conditions require continuity of normal stress across the interface, and continuity of normal displacement to the fluid interface. Since

[1] The second author discovered that κ, an additional non-dimensional coefficient that scales the cloud-radiative feedback and was defined in KE18 and E20, must be equal to 1 for consistency of the non-dimensional scaling.

the free troposphere is modeled as inviscid, the first condition simplifies to continuity of pressure:

$$\phi_s(x, y, z^* = 1, t) = \phi(x, y, p = \hat{p}_t, t). \tag{31}$$

Since there is no imposed shear across the tropopause, the second condition implies continuity of vertical velocity:

$$w_s^*(x, y, z^* = 1, t) = -B\omega(x, y, p = \hat{p}_t, t), \tag{32}$$

where $B = [(p_s - p_t)/p_t](H_s/H) > 0$ is a conversion coefficient between pressure coordinates and log-pressure coordinates.

c. Full, linear model

The troposphere system [Eqs. (14)–(17), (19)–(21)] is coupled to the stratosphere system [Eqs. (26)–(30)] through the two matching conditions [Eqs. (31) and (32)]. Altogether, these formulate a complete linear system, in which growing solutions whose energy decays to zero as $z^* \to \infty$ represent modes that grow in the troposphere and propagate vertically into the stratosphere.

3. Solutions

The full linear model is a complex system that cannot be easily solved theoretically. However, analyzing the model in the limits of 1) an inviscid surface with coupling to the stratosphere, and 2) a frictional surface under a rigid lid, allows us to isolate the impacts of both mechanisms. Solutions of the full model, with active surface friction and stratosphere coupling, are then analyzed to illuminate their combined effects.

a. Leaky modes

In this section, we focus first on solutions of the purely leaky modes, with no surface friction ($F = 0$). The solutions are analyzed separately: modes where $\upsilon = 0$ and higher-order meridional modes where there is nonzero meridional velocity. In what follows, unless otherwise stated, the primes are dropped from the linear perturbation variables.

1) $\upsilon = 0$ MODES

Although the full linear model is extremely complex, restricting the solutions to $\upsilon = 0$ allows for tractable analytical insight. In the troposphere, we assume solutions of the following form:

$$u_0 = \hat{U}_0(y)\exp(ikx + \sigma t), \tag{33}$$

where k is the zonal wavenumber, σ is the complex growth rate, and capitalized variables with hat notations are the meridional structure functions. Equivalent forms are assumed for ϕ_0, u_1, s, and s_m. Solutions in the stratosphere are assumed of the following form:

$$u_s = \frac{\hat{U}_s(y)}{\sqrt{\rho_0}}\exp\left[ikx + \sigma t + im(z^* - 1)\right], \tag{34}$$

where m is the complex vertical wavenumber. Equivalent forms are also assumed for ϕ_s, and w_s^*. As in KE18, the meridional structure of the $\upsilon = 0$ modes in the troposphere can be derived by combining Eqs. (14)–(17):

$$\frac{\partial}{\partial y}(\hat{S}^* - \hat{\Phi}_0) = \frac{iky}{\sigma}(\hat{S}^* - \hat{\Phi}_0). \tag{35}$$

Next, we combine Eqs. (14), (16), (20), and (21) to eliminate u_0, u_1, and s_m and obtain the relationship between the meridional function of the saturation moist entropy and the barotropic geopotential:

$$\hat{S}^* = \lambda\hat{\Phi}_0, \tag{36}$$

where

$$\lambda = \frac{ika_2 + k^2a_3}{\sigma a_1 + ika_2 + a_3k^2}, \tag{37}$$

$$a_1 \equiv D(1 + C) + (\chi + \sigma)(\gamma\sigma - C), \tag{38}$$

$$a_2 \equiv \alpha(\gamma\sigma + 1), \tag{39}$$

$$a_3 \equiv \gamma\sigma + (G - 1)C + G. \tag{40}$$

Combining Eqs. (35) and (36) gives us the meridional structure Y of the troposphere portion of the $\upsilon = 0$ modes:

$$Y = \exp\left(\frac{ik}{2\sigma}y^2\right), \tag{41}$$

which is equivalent in form to the meridional structure of the modes in the rigid-lid case. Furthermore, only solutions with an eastward phase speed satisfy the boundary conditions in y.

Next, we move on to solving the portion of the mode that exists in the stratosphere. With the solution form shown in Eq. (34), Eqs. (26)–(29) reduce to

$$\sigma\hat{U}_s + ik\hat{\Phi}_s = 0, \tag{42}$$

$$y\hat{U}_s + \frac{\partial\hat{\Phi}_s}{\partial y} = 0, \tag{43}$$

$$ik\hat{U}_s + \frac{m^2\sigma}{S}\hat{\Phi}_s = 0, \tag{44}$$

where $\hat{W}_s(y) = -(im\sigma/S)\hat{\Phi}_s(y)$, assuming $m^2 \gg (H/2H_s)^2$, which is a vertical shortwave approximation. Equations (42) and (44) combine into the well-known dispersion relation for the Kelvin wave:

$$\sigma = \pm i\frac{\sqrt{S}k}{m}. \tag{45}$$

As shown in Yano and Emanuel (1991), the associated group velocity is

$$c_{g,z} = \frac{k\sqrt{S}}{|m|^4}\left[\text{Real}(m)^2 - \text{Imag}(m)^2\right], \tag{46}$$

which indicates that the vertical group velocity increases with zonal wavenumber.

Next, Eqs. (42) and (43) combine to give a meridional structure that is equivalent to that of the troposphere shown in Eq. (41). For solutions that obey the meridional boundary conditions, or that the mode amplitudes go to zero as $y \to \pm\infty$, we must have that $\text{Imag}(\sigma) < 0$ (equivalent to an eastward phase speed), so we choose the positive root.

We now apply the matching conditions to derive the dispersion relation. The continuity of pressure condition demands that

$$\phi_s(x, y, z^* = 1, t) = \phi_0 - V_1(\hat{p}_t)s^*. \tag{47}$$

Equations (14) and (19) combine to give the vertical velocity at the tropopause in the troposphere, which must be equal to the vertical velocity at the tropopause in the stratosphere:

$$\omega(\hat{p}_t) = \frac{k^2}{\sigma}\,\phi_0 = -\frac{1}{B}\,w_s^* = \frac{1}{B}\,\frac{im\sigma}{S}\,\hat{\phi}_s, \tag{48}$$

where we note the equivalence of a rigid lid $[\omega(\hat{p}_t) = 0]$ to the absence of the barotropic mode. Combining with Eqs. (10), (36), (45), and (47), Eq. (48) reduces to the dispersion relation:

$$\underbrace{\sigma a_1 + a_4}_{\text{rigid lid}} + \underbrace{\sigma(kB\sqrt{S})^{-1}(\sigma a_1 + \nu a_4)}_{\text{correction}} = 0, \tag{49}$$

where $\nu = 1 - V_1(\hat{p}_t)$ and $a_4 = ika_2 + a_3k^2$. As shown in the underbraces, Eq. (49) is written in the form of the rigid-lid dispersion relation, plus a quartic-order correction term whose magnitude is inversely proportional to the square root of the stratosphere stratification, S. It is clear that in the limit of $S \to \infty$, the dispersion relation reduces to that of the rigid-lid case. The quartic dispersion relation is solved numerically and the solutions are checked rigorously to satisfy the governing equations, boundary conditions, and matching conditions.

Before examining the solutions of the leaky $\nu = 0$ modes, we first briefly derive the functional form of ω in the troposphere, in the case where $\nu = 0$. We start by taking the time derivative of the non-dimensional continuity equation and substitute the zonal velocity using Eqs. (14) and (16):

$$\sigma\frac{\partial\omega}{\partial\hat{p}} = k^2\phi. \tag{50}$$

Taking a derivative in pressure allows us to substitute in Eq. (3) and yields

$$\sigma\frac{\partial^2\omega}{\partial\hat{p}^2} = -k^2\left(\frac{\partial T}{\partial\hat{p}}\right)_{s^*}s^*. \tag{51}$$

Integrating in pressure once returns

$$\sigma\frac{\partial\omega}{\partial\hat{p}} = -k^2s^*\overline{T}(\hat{p})\big|_{s^*} + C_0, \tag{52}$$

where C_0 is an integration constant that must be determined through the boundary conditions. We integrate from the surface to the tropopause:

$$\sigma(\omega(\hat{p}_t) - \omega(\hat{p}_s)) = (\hat{p}_s - \hat{p}_t)(-k^2s^*[\overline{T}] + C_0), \tag{53}$$

which allows us to determine C_0:

$$C_0 = \sigma\frac{\omega(\hat{p}_t) - \omega(\hat{p}_s)}{\hat{p}_s - \hat{p}_t} + k^2s^*[\overline{T}]. \tag{54}$$

Substituting for C_0 into Eq. (52), setting $\omega(\hat{p}_s) = 0$ as earlier, and integrating once in pressure yields the non-dimensional vertical structure of ω:

$$\omega(\hat{p}) = \underbrace{\frac{\hat{p}_s - \hat{p}}{\hat{p}_s - \hat{p}_t}\,\omega(\hat{p}_t)}_{\text{barotropic}} - \underbrace{\frac{k^2}{\sigma}\,s^*\int_{\hat{p}_s}^{\hat{p}} V_1\,d\hat{p}}_{\text{baroclinic}}. \tag{55}$$

As shown in the underbraces, the vertical structure of the pressure vertical velocity is a sum of the barotropic and baroclinic modes. The barotropic component changes linearly with pressure, and the baroclinic mode is zero at the surface/tropopause and peaks in the midtroposphere. The superposition of the barotropic and baroclinic mode can lead to a vertical tilt in the vertical velocity profile that depends on the phase lag between the two modes. It is worth noting that by definition, the baroclinic mode cannot interact with the stratosphere; in this model, it is only through the excitement of the barotropic mode that waves can radiate energy into the stratosphere.

Figure 1 compares the non-dimensional frequency, growth rates, phase speeds, and vertical group velocity of the leaky $\nu = 0$ modes to those of the rigid-lid modes, with non-dimensional coefficients $\alpha = 1.5$, $\chi = 0.5$, $C = 0$, $\gamma = 2$, $D = 0.5$, $G = 0.1$, and $S = 100$. These parameters somewhat reflect Earth-like conditions in the tropics, with the exception of no cloud radiation interaction, and were specifically chosen to examine the branch of solutions that closely resemble the classical Kelvin-wave solutions but are instead amplified through the WISHE feedback. Figure 1a shows that the frequencies of the leaky waves are only slightly larger than their rigid-lid counterparts, and as such the phase speeds are slightly faster (Fig. 1c). The modification of the growth rates tell a much different story: Fig. 1b shows strong damping of the growth rate of smaller-scale waves, shifting the power spectrum toward larger scale waves, which is consistent with the results of Yano and Emanuel (1991). This reddening of the power spectrum can be physically explained through the large vertical group velocities of the smaller scale waves, as shown in Fig. 1c and indicated in Eq. (46). The smaller scale waves propagate their energy very quickly into the stratosphere, dampening their growth rate. For instance, the $k = 10$ wave has a vertical group velocity that nearly exceeds its zonal phase speed.

Figure 2 shows a summary of the $k = 1$ eigenfunction using identical non-dimensional parameters as detailed in Fig. 1. The horizontal cross section at the surface shows a Kelvin wave pattern with surface easterlies maximizing east of the

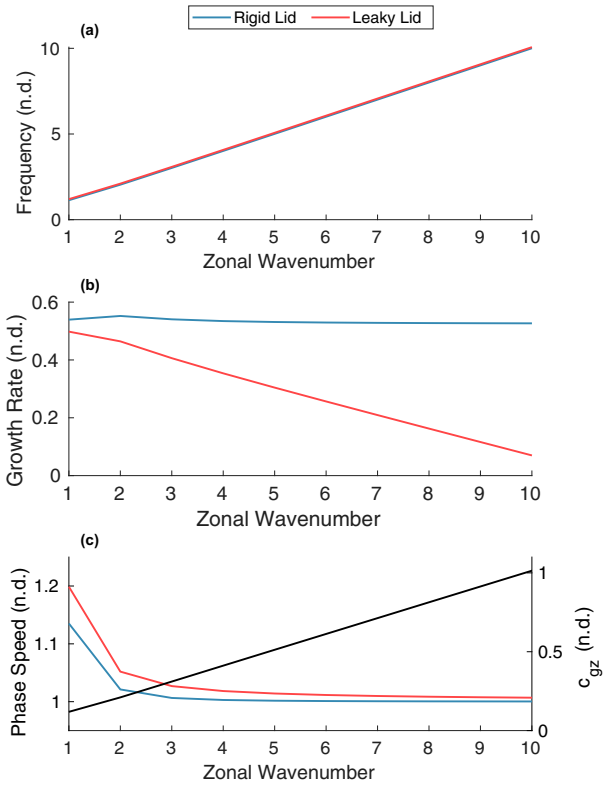

FIG. 1. Non-dimensional (a) frequency, (b) growth rate, and (c) phase speed and for the fastest-growing $v = 0$ mode. Vertical group velocity of the leaky mode is shown in black in (c), while rigid-lid solutions are shown in blue and leaky-lid solutions shown in red. Non-dimensional parameters are $\alpha = 1.5$, $\chi = 0.5$, $C = 0$, $\gamma = 2$, $D = 0.5$, $G = 0.1$, and $S = 100$.

maximum temperature anomaly. Vertical velocity maximizes west of the peak temperature anomalies, and the WISHE feedback is responsible for wave growth and enhanced eastward propagation. The horizontal structure is not significantly modified from that of the rigid lid. The vertical structure of the mode exhibits a bit more complexity. Unlike the vertical structure of the rigid-lid model, which is purely baroclinic, the superposition of the barotropic and baroclinic modes leads to an eastward vertical tilt in dynamical fields, as shown in Fig. 2 and Eq. (55). Note the temperature anomalies are purely first baroclinic, since the barotropic mode is not associated with temperature perturbations The mode has a downward phase propagating, eastward tilted component in the stratosphere, which is consistent with a Kelvin-wave that has upward vertical energy propagation. As indicated by the dispersion relation, the vertical wavelength in the stratosphere is controlled by the horizontal wavenumber and stratification; a stronger stratification or shorter horizontal wavelength decreases the vertical wavelength.

The tropospheric system also allows for solutions of significantly slower propagating modes when cloud-radiation interaction is turned on, as shown in KE18 and E20. We select the non-dimensional parameters $\alpha = 1$, $\chi = 1$, $C = 2.5$, $\gamma = 2$, $D = 1$, $G = 0.02$, and $S = 100$, in order to obtain the slow modes as the fastest-growing solutions. Note that these parameters are slightly different from those used in E20, but still within Earth-like ranges. The use of slightly different parameters was motivated in part to compensate for the recognition that $\kappa = 1$. We also eliminated horizontal diffusion of moist static energy as compared to the model described in KE18, in order to isolate the effect of the stratosphere on the growth rates. This means that the growth rates no longer peak at low wavenumbers, contrary to what is observed, suggesting that horizontal advection may play an important role in scale-selection for slow-propagating waves. We have confirmed that the different non-dimensional parameters used and the removal of the horizontal diffusion term does not change the general structure and properties of the slow-propagating waves (not shown). Figure 3 shows the frequency, growth rate, phase speed, and vertical group velocities for the $v = 0$ slow modes that

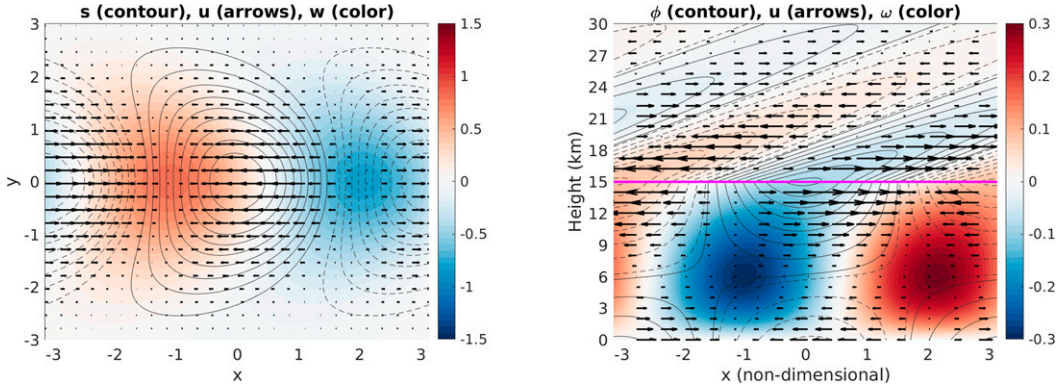

FIG. 2. Eigenfunction of the $v = 0$, $k = 1$ mode corresponding to the parameters detailed in Fig. 1, on (left) a horizontal cross section at the surface and (right) a vertical cross section centered on the equator. Contours indicate the saturation entropy or geopotential, where solid (dashed) lines indicate positive (negative) perturbations. Arrows indicate zonal velocity perturbations, and color shading indicates vertical velocity or ω perturbations, where indicated. Magenta line outlines the tropopause.

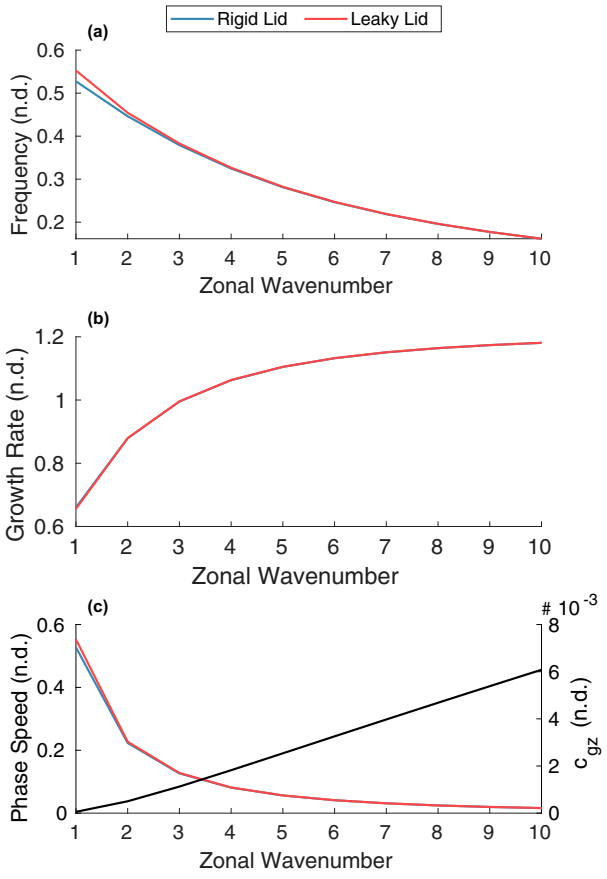

FIG. 3. As in Fig. 1, but for the fastest-growing mode with non-dimensional parameters $\alpha = 1$, $\chi = 1$, $C = 2.5$, $\gamma = 2$, $D = 1$, $G = 0.02$, and $S = 100$.

can interact with the stratosphere. Aside from a small modification of the wave properties at the highest wavenumbers, these slow modes are not significantly affected by the presence of a stratosphere. Their vertical group velocities are almost negligibly small, and the corresponding vertical wavelengths in the stratosphere are extremely short. These slow modes are trapped in the troposphere and do not leak much energy into the stratosphere. Thus, these results suggest that for slow-propagating modes, such as the MJO, a rigid-lid assumption is an accurate approximation with regards to the growth rates.

Next, we investigate the barotropic mode magnitude and phase tilt across a range of non-dimensional parameters. Combining Eqs. (14), (16), and (36) under $\upsilon = F = 0$ yields the relationship between the baroclinic and barotropic zonal velocities:

$$-\lambda u_0 = u_1. \tag{56}$$

Here, it is evident that λ controls the phase and amplitude relationship between the barotropic and baroclinic modes. From Eq. (56), the ratio of the amplitude of the barotropic to that of the baroclinic mode is equivalent to $|-\lambda^{-1}|$, while the phase lead of the barotropic to baroclinic mode is given by $\tan^{-1}(\lambda_i/\lambda_r)$, where λ_i and λ_r are the imaginary and real components of λ, respectively. It follows that the barotropic zonal velocity to total zonal velocity ratio is $|u_0/(u_0 + u_1)| = |(\lambda - 1)^{-1}|$.

Figures 4a and 4c show the barotropic zonal velocity to total zonal velocity ratio, as well as the phase lead of the barotropic mode to the baroclinic mode, for a wide range of stratosphere stratification S. In general, we observe decreasing amplitude of the barotropic mode with increasing stratosphere stratification and zonal wavenumber. For both the classical WISHE-driven Kelvin waves (Fig. 4, top row) and radiatively destabilized slow modes (Fig. 4, bottom row), the barotropic mode is around an order of magnitude smaller than the baroclinic mode for Earth-like parameters. Furthermore, the barotropic mode leads the baroclinic mode by approximately 0.1–0.2 cycles (0.25 being a quarter cycle, or $\pi/2$). The phase lead of the barotropic mode is always positive, indicating that the eastward phase tilt in dynamical fields shown in Fig. 2 is robust across a wide-range of scales and S. In addition, an exploration of the non-dimensional parameter space did not find any solutions where the barotropic mode lagged the baroclinic mode (not shown). This result is consistent with physical intuition. For the WISHE-driven $\upsilon = 0$ modes, the baroclinic easterlies peak east of the maximum temperature perturbation. If the barotropic zonal velocities are instead westward of the baroclinic zonal velocities, then the total surface easterlies could peak west of the maximum temperature anomalies, which is inconsistent with a WISHE-driven eastward-propagating mode. Note, this is inconsistent with observational analyses of convectively coupled Kelvin waves, in which a westward tilts with height in zonal wind and temperature are typically observed (Straub and Kiladis 2002). But, an explanation of the westward tilt with height in *temperature* is futile to search for in a strict quasi-equilibrium model, since the barotropic mode is not associated with temperature perturbations. Rather, this analysis shows that the barotropic mode, at least in WISHE-amplified Kelvin waves in which quasi-equilibrium restricts the vertical structure of buoyancy anomalies, is eastward of the first baroclinic mode. Regardless, the observed westward tilt with height in temperature may indeed indicate the importance of the second baroclinic mode over the barotropic mode for Kelvin waves (Mapes 2000; Kuang 2008a), though it is also possible to obtain the observed tilt with height in temperature in simple models where a first-baroclinic mode heating rate is imposed and convective inhibition is allowed to modulate precipitation (Raymond and Fuchs 2007). It is likely true that strict quasi-equilibrium, as employed in this study, is too restrictive an assumption for the fast-moving Kelvin waves, but relaxation of this assumption in a coupled troposphere–stratosphere model is beyond the scope of this study.

Finally, it is worth noting that the u_0 magnitude is larger than the u_1 magnitude for extremely leaky stratospheres (Fig. 4); though this may not be relevant to Earth's atmosphere, a barotropic mode that exceeds its baroclinic counterpart leads to top-heavy vertical velocity profiles and fast propagation into the stratosphere.

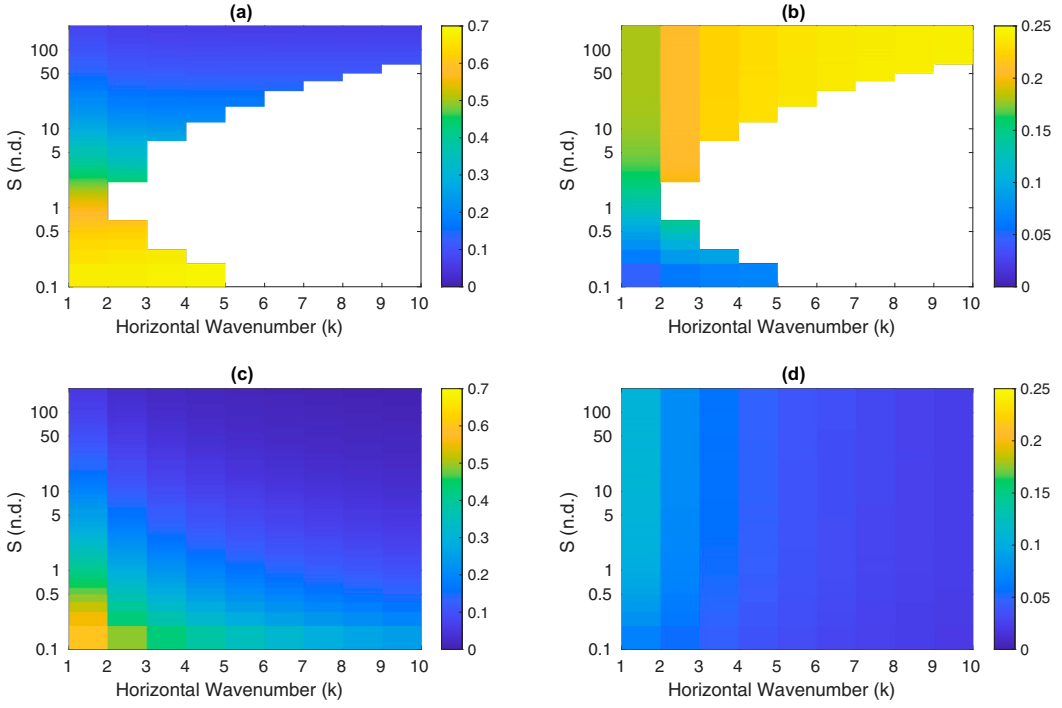

FIG. 4. (a),(c) Barotropic zonal velocity to total zonal velocity ratio $[|u_0/(u_0 + u_1)| = |(\lambda - 1)^{-1}|]$, and (b),(d) phase lead of the barotropic mode with respect to the baroclinic mode $[\tan^{-1}(\lambda_i/\lambda_r)]$, in cycles, as functions of stratosphere stratification S and horizontal wavenumber. The plots in (a) and (b) are Generated using the non-dimensional parameters described in Fig. 1 (WISHE-modified Kelvin waves), and the plots in (c) and (d) are generated using the non-dimensional parameters described in Fig. 3 (slow $v = 0$ modes). White area indicates non-growing modes.

2) HIGHER-ORDER MODES

Without the $v = 0$ approximation, the solution set is extremely complex. In the rigid-lid case, the meridional structure of the eigenmodes of the full equations are parabolic cylinder functions of degree n, where n is the order of the Hermite polynomial. A brief mathematical analysis of the (intractable) leaky-lid solutions suggests that the meridional structure functions of the linear solutions are sums of parabolic cylinder functions. Note that by convention, we denote $n = -1$ solutions as those where $v = 0$.

For these higher-order modes, we instead solve the linear problem using numerical code, which is only appropriate for finding growing modes. The troposphere system [Eqs. (14)–(17), (20)–(21)] is discretized in y, while the stratosphere system [Eqs. (26)–(29)] are discretized in y and z. Solutions are assumed to have a zonal structure of the form $\exp(ikx)$. To integrate the linear system in time, the stratosphere equations need to be transformed to a set of linear prognostic equations. The mass continuity equation [Eq. (28)] is first integrated from the lower boundary in z^*, to obtain

$$\rho_s w_s^*(y, z^*) = w_s^*(y, z^* = 1) - \int_{z^*=1}^{z} \left\{ \rho_s \left[iku_s(y, z^*) + \frac{\partial}{\partial y} v_s(y, z^*) \right] \right\} dz^*, \quad (57)$$

where the tropopause velocity $w^*(z^* = 1)$ is equal to the vertical velocity at the tropopause in the troposphere equations, as required from the vertical velocity matching condition. Given the vertical velocity, Eq. (29) can be used to calculate the geopotential:

$$\frac{\partial}{\partial t} \frac{\partial}{\partial z} \phi(y, z^*) = -w^*(y, z) S. \quad (58)$$

Integrating from the upper boundary downward gives the prognostic equation for ϕ_s:

$$\frac{\partial}{\partial t} \phi_s(y, z^*) = -\int_{\infty}^{z} w_s^*(y, z^*) S \, dz^* + C_0, \quad (59)$$

where C_0 must be determined by the upper boundary condition. An upward wave radiation boundary condition could be applied to determine C_0, as in Moskowitz and Bretherton (2000), but such a condition does not exist for the slower modes that have interactive cloud radiation and no clear analog in the stratosphere. While it is not necessary that $\phi_s = 0$ as $z \to \infty$ (as long as the energy density goes to zero), we have included a Newtonian damping in a sizeable layer extending from the upper boundary, and as such, we set $C_0 = 0$. Another advantage of the Newtonian damping in the upper part of the domain is to eliminate any nonphysical downward-propagating modes. For realistic values of S, however, the amplitude of the modes typically decay to zero at the top of the numerical domain. Finally, $\phi_s(y, z^* = 1)$ is connected to

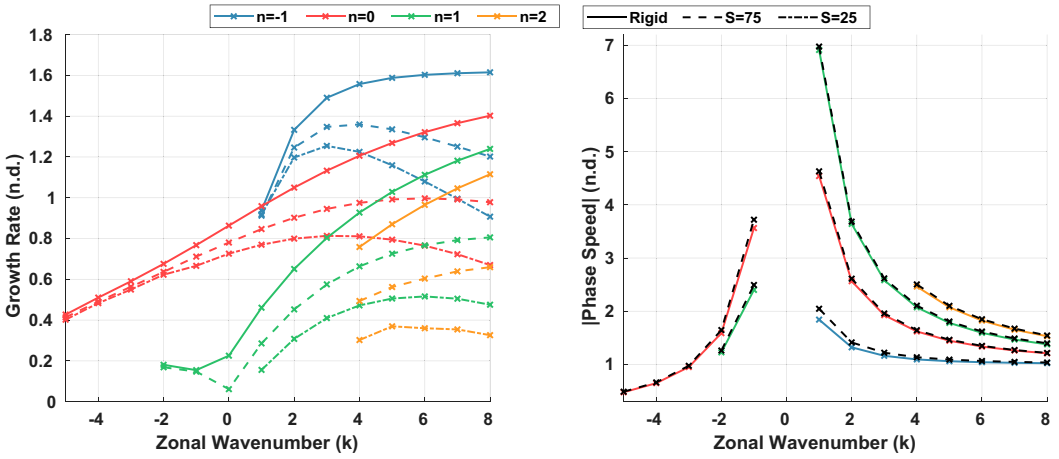

FIG. 5. (left) Non-dimensional growth rate for the $n = -1, 0, 1, 2$ modes of the rigid-lid system (solid), the leaky-lid system with $S = 75$ (dashed), and the leaky-lid system with $S = 25$ (dot–dashed). (right) Non-dimensional phase speed for the same modes, in the rigid-lid (solid) and leaky-lid system with $S = 75$ (black dashed). We omit $k \leq 3$ for $n = 2$ and $k \leq 0$ for $n = 1$ for $S = 25$ solutions since they do not grow rapidly enough to infer the complex growth rate. Non-dimensional parameters selected for these modes are $\alpha = 3.5$, $\chi = 0.5$, $C = 0$, $\gamma = 1$, $D = 2.5$, $G = 0.25$, and $\delta_x = 15$.

the troposphere through the continuity of pressure matching condition [Eq. (47)].

Spatial derivatives are approximated using fourth-order central differences, and the system is forward time-stepped using fourth-order Runge–Kutta. After specifying non-dimensional parameters, the corresponding rigid-lid solution is used to initialize the troposphere domain, while the stratosphere is initialized at rest. Since the unbalanced wave must undergo rapid gravity wave adjustment, several dampening mechanisms are used to eliminate spurious gravity wave energy. A spectral filter is applied at each time step to eliminate small-scale noise. A strong sponge-layer is included along the edges and top of the domain to eliminate reflection of gravity waves, downward-propagating waves, and spurious noise. For details on the mathematical form of the full numerical system, see appendix A. The system is integrated for a long period of time, during which the domain is periodically rescaled by a constant to prevent numerical overflow. We then isolate the growing mode of interest and infer both the complex growth rate and meridional/vertical structures. The real component of the growth rate is calculated by the linear slope of the time-varying log of the amplitude of a prognostic variable (after accounting for the rescaling). The imaginary component of the growth rate is calculated by the slope of the time-varying phase of a prognostic variable. Although we initially assume that the damping at the upper boundary does not significantly affect the stratospheric solution, the corresponding growth rate and the meridional structures of all prognostic variables are rigorously checked to satisfy the governing equations, boundary conditions, and matching conditions. As a partial test of correctness of the numerical code, the numerical solutions for the $v = 0$ ($n = -1$) modes were cross referenced with the $v = 0$ analytic solutions.

The numerical solution is robust for linear solutions that are the fastest-growing equatorially symmetric or asymmetric mode. However, for solutions that are not the fastest-growing mode, initial unbalanced energy and/or numerical error that projects onto the fastest-growing mode symmetric/asymmetric mode will cause the slower growing mode to be overtaken by the fastest-growing mode before the domain energy is concentrated solely in the mode of interest. For instance, the second-fastest-growing equatorially symmetric mode can be overtaken by the fastest-growing equatorially symmetric mode. In these cases, the meridional–vertical structure of the fastest-growing mode is isolated by integrating for a long period in time. Then, the fastest-growing mode is projected onto the domain output, and removed from the fields. If the second-fastest-growing mode does not have a weak growth rate, the remaining, filtered fields will contain the mode of interest for a long enough period of time to infer the complex growth rate and structure.

(i) WISHE classical modes

We first compare the leaky wave solutions to the rigid-lid solutions for the WISHE-destabilized classical modes of the equatorial waveguide. This is done by choosing $\alpha = 3.5$, $\chi = 0.5$, $C = 0$, $\gamma = 1$, $D = 2.5$, $G = 0.25$, $\delta_x = 15$, and $S = 75$; note that $C = 0$ eliminates the slower propagating modes observed in KE18 and E20. Figure 5 shows the non-dimensional growth rates and phase speeds for select meridional orders $n = -1, 0, 1, 2$ leaky equatorial waves. The growth rates of the Kelvin, westward and eastward mixed Rossby–gravity, and inertia–gravity waves are clearly dampened in relation to their rigid-lid counterparts. The strength of dampening, in a percent relative sense, grows stronger with increasing wavenumber for the eastward modes. This is in contrast to the almost negligible dampening of the

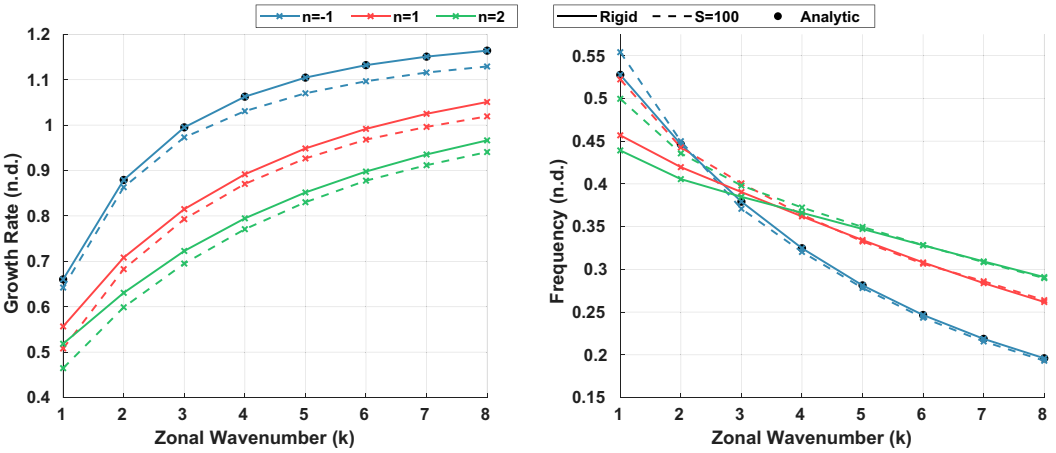

FIG. 6. (left) Non-dimensional growth rate for the $n = -1, 1, 2$, eastward-propagating slow modes of the rigid-lid system (solid) and the leaky-lid system with $S = 100$ (dashed) inferred from the numerical solution. (right) Non-dimensional frequency for the same modes, in the rigid-lid (solid) and leaky-lid system with $S = 100$ (dashed). Black dots indicate the analytic solutions of the growth rate and frequencies of the $n = -1$ slow modes. All $n = 0$ solutions are not growing. Non-dimensional parameters selected for these modes are $\alpha = 1$, $\chi = 1$, $C = 2.5$, $\gamma = 2$, $D = 1$, $G = 0.02$, and $\delta_x = 30$.

westward-propagating modes as $|k|$ increases. The growth rates of the westward-propagating $n = 0$ and $n = 1$ waves are not strongly affected by the stratosphere. The phase speeds of the leaky waves are almost negligibly faster than their rigid-lid counterparts, with the largest, though still slight, modifications observed for the $n = -1$ solutions. The growth rates for smaller scale eastward-propagating waves are further dampened with reduced stratification in the stratosphere (cf. $S = 75$ and $S = 25$). The effect is quite pronounced; in the case shown in Fig. 5, the smallest scale rigid-lid modes possess the largest growth rates, but imposing a leaky stratosphere greatly shifts the growth rates toward larger scales. For the $S = 25$ case, the growth rate peaks at $k = 3$ for the $n = -1, 0$ modes, and $k \approx 5$ for the $n = 1, 2$ modes. These results are consistent with the qualitative behavior shown in the mathematical analysis of the leaky $v = 0$ modes. As such, the solutions suggest that the stratosphere acts as a reddener of the equatorial power spectrum, especially for eastward-propagating waves.

(ii) Slow modes

We next switch to a non-dimensional parameter set in which cloud radiative feedbacks are turned on, such that the slow modes analyzed in E20 are the fastest-growing modes. In particular, we choose $\alpha = 1$, $\chi = 1$, $C = 2.5$, $\gamma = 2$, $D = 1$, $G = 0.02$, $\delta_x = 30$, and $S = 100$. Although the westward-propagating slow modes do grow in time under the rigid-lid model, they take too long to reach a steady state and are quickly overtaken by the eastward-propagating modes. We thus focus on the eastward-propagating slow modes, which have a much clearer analog in the real atmosphere (i.e., the MJO).

Figure 6 shows the non-dimensional growth rates and frequencies for the eastward-propagating $n = -1, 1, 2$ slow modes. We first compare the numerical $n = -1$ solutions to the analytic solutions (Fig. 6, black dots). We observe that the numerical model slightly dampens the growth rate, and only negligibly modifies the frequencies. This slight damping could be attributed to the spectral filter and/or numerical error. Assuming that the numerical error affects the wave characteristics of the $n = 1, 2$ slow modes the same way, we can infer that like the growth rates and frequencies of the leaky $n = -1$ slow modes, the growth rates and phase speeds of the higher-order slow modes are not affected by the presence of the stratosphere.

Perhaps of greater interest is how the slow modes interact with the stratosphere through the barotropic mode. We focus on the eastward-propagating $n = 1$, $k = 2$ mode, which has a horizontal structure that closely resembles that of the observed MJO (Emanuel 2020). Figure 7 shows the horizontal and vertical structure of the $n = 1$, $k = 2$ mode, where we observe surface cyclonic gyres westward and poleward of the area of maximum ascent. Strong westerlies are also observed westward of the maximum ascent region. The boundary layer horizontal structure very closely resembles that of the rigid-lid solution (not shown). At the tropopause (Fig. 7, top right), the horizontal structure is almost nearly the opposite of the horizontal structure at the surface, indicating the prominence of the first baroclinic mode. However, the vertical velocity at the tropopause is nonzero, and the pattern extends poleward into the cyclonic/anticyclonic gyres, an indication of the presence of the barotropic mode. If we move further up into the stratosphere, at around 20 km (Fig. 7, bottom left), the signature of the equatorial portion of the tropospheric wave disappears, and the poleward cyclonic/anticyclonic gyres become the prominent pattern. These gyres have a westward tilt with height, as indicated in the vertical cross section at $y = 2.5$ (Fig. 7, bottom right), though their amplitudes decay exponentially with height and are much smaller with respect to the amplitudes of the

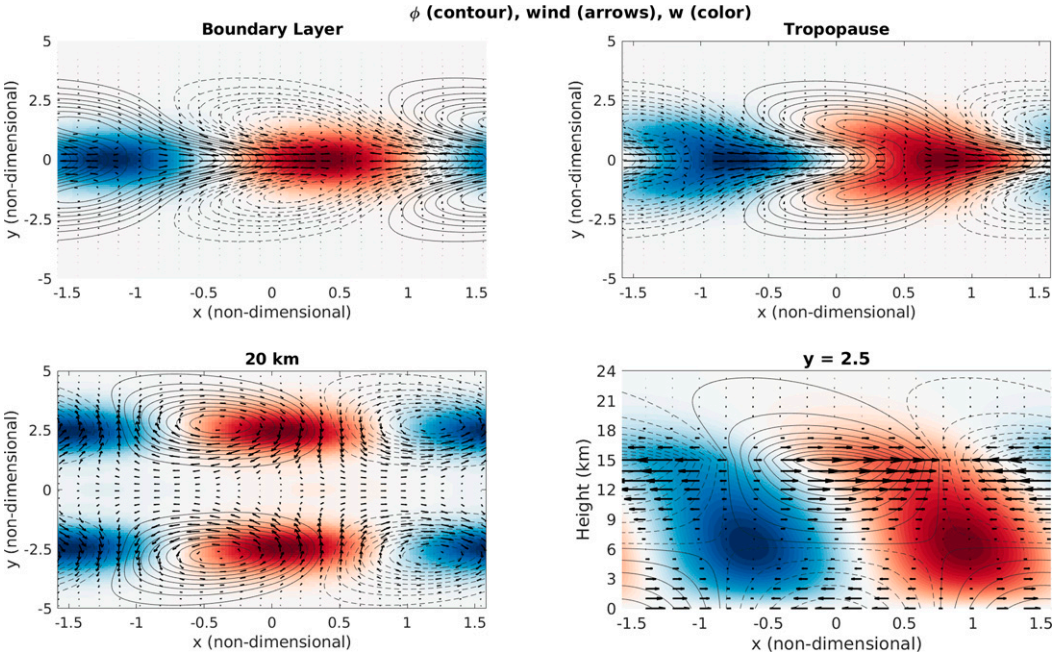

FIG. 7. Eigenfunction of the $n = 1$, $k = 2$ mode corresponding to the parameters detailed in Fig. 6, on a horizontal cross section at the (top left) the surface, (top right) tropopause (15 km), and (bottom left) 20 km. (bottom right) Vertical cross-section eigenfunction at $y = 2.5$. Contours indicate the geopotential, where solid (dashed) lines indicate positive (negative) perturbations. Arrows indicate wind perturbations, and color shading indicates vertical velocity perturbations at the level indicated, except for the boundary layer cross section, where color shading indicates midlevel vertical velocity.

corresponding gyres in the troposphere. This indicates that the barotropic mode lags the baroclinic mode; in addition, the westward tilt height observed here is consistent with an upward-propagating Rossby wave. At the equator, the $n = 1$, $k = 2$ slow mode has a very weak eastward tilt with height (not shown), since the barotropic mode leads the baroclinic mode. Like the $v = 0$ mode shown in Fig. 2, in the stratosphere, the slow mode also tilts eastward with height at the equator (not shown). This is consistent with the stratospheric eastward tilt with height of the zonal wind on the equator of observational MJO composites [see Fig. 3 of Kiladis et al. (2005)].

b. Frictionally modified modes

In this section, we consider how surface friction can also excite the barotropic mode. First, we simplify the linear system in the rigid-lid limit, but now with nonzero surface friction. From Eq. (19), if $\omega(\hat{p}_t) = 0$, it follows that the barotropic mode is nondivergent. However, the solution cannot be solved in terms of a nondivergent streamfunction ψ_0, since δ_x scales the meridional momentum equation but not the mass continuity equation. Instead, we take the divergence of Eqs. (14) and (15), yielding

$$\left(\delta_x \frac{\partial^2}{\partial y^2} - k^2\right)\phi_0 = y\left(ikv_0 - \delta_x \frac{\partial u_0}{\partial y}\right) - \delta_x u_0 - 2Fik(u_0 + u_1) - F\frac{\partial}{\partial y}(v_0 + u_1). \quad (60)$$

From Eq. (60), we see that a barotropic mode at rest cannot be excited if there is no surface friction ($F = 0$). Thus, surface friction acts to couple the barotropic mode with the baroclinic mode; since the forcing is primarily in the first baroclinic mode; it is the first baroclinic mode that excites the barotropic mode.

The barotropic geopotential ϕ_0 is solved by inverting Eq. (60). Equations (14)–(17), (20), and (21) form the complete linear system. The system is solved numerically by discretizing in y. Spatial derivatives are again approximated using fourth-order central differences, and the system is forward time-stepped using fourth-order Runge–Kutta. As before, the frictionless, rigid-lid solution is used to initialize the domain, after which we integrate the system for a long period of time and then isolate the growing mode of interest.

Before proceeding, it is important to note that the $n = -1$ modes in this section differ from the traditional definition of $v = 0$, in that the meridional wind is allowed to be nonzero but small. This is deliberately chosen, since $v_0 = v_1 = 0$ solutions under zero vertical velocity boundary conditions require the barotropic mode to be divergence free; this is only achievable for nonzero u_0 if there are also nonzero v_0. While solutions of $v_0 = v_1 = 0$ under the aforementioned conditions do exist, they are just classical frictionally damped baroclinic mode solutions. However, we are interested in the solutions in which the barotropic mode can be excited, and as such, allow v to be small for the $n = -1$ modes. We investigate the complex growth rates as a function of the non-dimensional surface

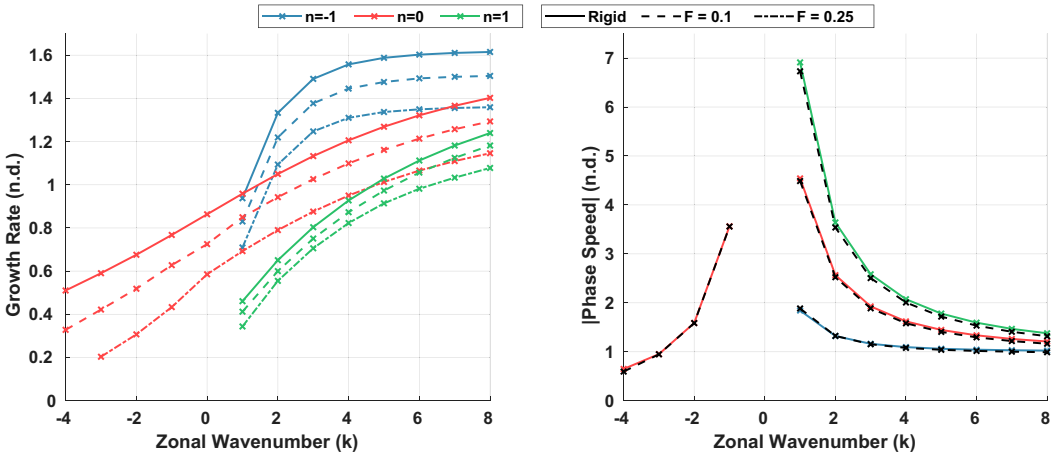

FIG. 8. (left) Non-dimensional growth rate for the $n = -1$, 0, 1 modes of the rigid-lid system (solid), the surface friction + rigid-lid system with $F = 0.1$ (dashed), and the surface friction + rigid-lid system $F = 0.25$ (dot–dashed). The $n = -1$ modes differ from the traditional definition of $v = 0$, in that the meridional wind is allowed to be nonzero but small. (right) Non-dimensional phase speed for the same modes, in the rigid-lid (solid) and surface friction + rigid-lid system with $F = 0.1$ (black dashed). All $n = 2$ and the $n = 1$ for $k \leq 0$ solutions are omitted since they do not grow rapidly enough to infer the complex growth rate. Non-dimensional parameters selected for these modes are $\alpha = 3.5$, $\chi = 0.5$, $C = 0$, $\gamma = 1$, $D = 2.5$, $G = 0.25$, and $\delta_x = 15$.

friction, F, for which an Earth-like range is $F \approx 0.1$–0.4. Figure 8 shows the growth rate of the $n = -1$, $n = 0$, and $n = 1$ modes for the same parameter choices as in Fig. 5, which selects for WISHE-modified Matsuno modes. Figure 8 indicates that the surface friction acts as a damping effect on all wavelengths, and the strength of the damping is nearly constant across all wavelengths. This is expected as the aerodynamic drag law acts on a fixed damping time scale. The phase speeds are not significantly changed from the phase speeds of the rigid-lid modes. The results are consistent with our formulation of surface friction, in that surface friction does not "force convection," as convection is assumed to be in a strict, statistical equilibrium.

As illustrated in Eq. (60), surface friction can lead to an excitation of the barotropic mode, even under a rigid lid. Figures 9a and 9b show the meridional structure of the $n = -1$, $k = 1$ barotropic zonal and meridional velocities as compared to their baroclinic counterparts. Like the leaky-lid case, the barotropic zonal wind magnitude is around an order of magnitude smaller than the baroclinic mode. However, while the baroclinic mode magnitudes are primarily confined close to the equator (around $y = -5$ to $y = 5$), the barotropic mode wind velocities have long tails that extend far away from the equator. To understand this effect, at least on a high level, we consider neutral barotropic and baroclinic equatorial waves. Since a neutral barotropic wave will have a larger phase speed (and equivalent depth) than a neutral baroclinic wave, it will consequently have a larger meridional length scale and a more poleward turning latitude [see Eq. (8.77) in Vallis (2017)]. This qualitatively explains the increased poleward extent of the barotropic mode as compared to the baroclinic mode. A more quantitative discussion, under the simplest possible dynamics, is discussed in appendix B. The barotropic mode might be an important teleconnection mechanism between the tropics and the extratropics, but further analysis of this effect is out of the scope of this study (Horel and Wallace 1981). An important caveat to note, however, is that a rigid-lid barotropic mode is completely trapped in the troposphere; the addition of a leaky stratosphere may limit the poleward extent of the barotropic mode, as will be examined in the next section.

Under a rigid lid the nondivergent barotropic mode cannot be associated with vertical velocity perturbations, though a vertical tilt can still exist in the horizontal wind fields from the superposition of the barotropic and baroclinic horizontal winds. Figure 9d shows the vertical cross section on the equator of the $n = -1$, $k = 1$ mode. The vertical structure of the vertical velocity is only first baroclinic, despite the zonal wind exhibiting a slight eastward vertical tilt. This eastward vertical tilt in the zonal wind field is consistent with the eastward tilt observed in the purely leaky $n = -1$ modes. This is because the barotropic mode leads the baroclinic mode, as can also be seen in the horizontal structure of the boundary layer vorticity decomposition in Fig. 9c.

Unfortunately the numerical model is quite unstable for the slow modes in the rigid-lid, surface friction limit. Despite strong sponge layers, instabilities unrelated to the slow modes (spurious noise, gravity waves) develop quickly in the numerical domain, precluding inferral of the complex growth rate and horizontal structure. The behavior of the barotropic mode in the slow modes will be discussed in the following section using the fully coupled, surface friction model, albeit with a large stratosphere stratification, instead of a rigid lid.

These results show that surface friction act strictly as a damping mechanism in our framework, contrary to the results shown in Moskowitz and Bretherton (2000). This is likely

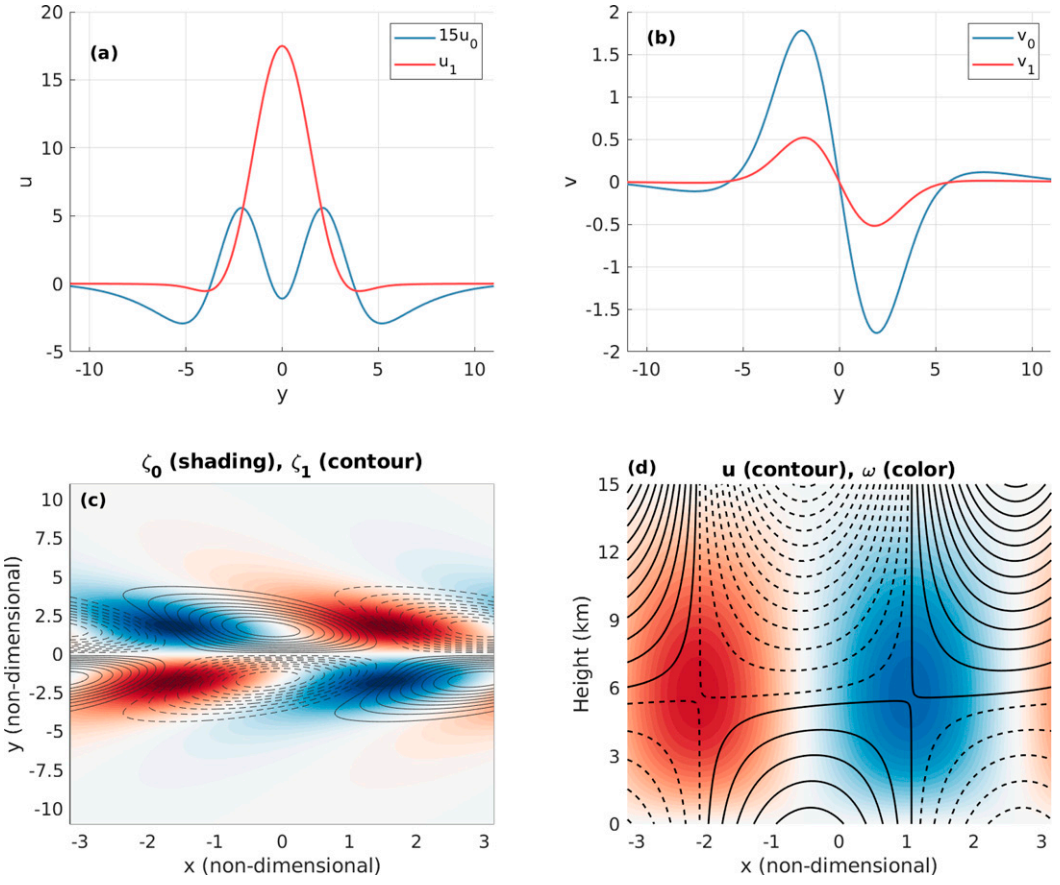

FIG. 9. (a) Meridional structure of 15 times the barotropic zonal wind and the baroclinic zonal wind for the $n = -1, k = 1$ mode with $F = 0.25$ and the parameter set chosen in Fig. 8. (b) As in (a), but for the barotropic and baroclinic meridional wind. (c) Horizontal structure of the boundary layer barotropic vorticity (shading) and baroclinic vorticity (contours). (d) Equatorial vertical cross sections of the pressure vertical velocity (shading) and zonal wind perturbations (contours) for the same mode. Solid (dashed) contours are positive (negative) zonal wind anomalies.

because the convective heating associated with frictional convergence cannot "force" the system, as convection must be balanced by adiabatic cooling from large-scale subsidence and downdrafts that import low entropy midlevel air into the boundary layer. Surface friction does, however, act to modify both the horizontal and vertical structure of the equatorial waves, as shown through the long poleward tails of the barotropic mode and vertical tilt in the zonal wind fields.

c. Leaky, frictionally modified modes

While examining the excitation of the barotropic mode in the limits of surface friction under a rigid lid and a frictionless surface under a leaky lid were both useful exercises to isolate their respective effects on tropical waves, in the real world, both surface friction and leakage of energy to the stratosphere can act simultaneously to modify equatorial waves through excitation of the barotropic mode. In particular, the long tails of the tropospherically trapped barotropic mode observed in the rigid lid, surface friction model may behave differently if the barotropic mode can leak energy into the stratosphere.

To understand the extent to which both of these mechanisms can interact, we run the full troposphere–stratosphere numerical model with nonzero surface friction, using the same methods to infer the complex growth rates and eigenmodes. We first examine their combined effect on the WISHE-driven classical Matsuno modes through the same parameter set as used in Figs. 5 and 8. In addition, we focus on the eastward-propagating modes since the westward-propagating modes were not strongly affected by the presence of the stratosphere.

Figures 10a and 10b show the non-dimensional growth rate and phase speeds for the WISHE destabilized Matsuno modes, respectively. Since there is both energy leakage into the stratosphere and surface friction, the growth rates are strongly dampened from the equivalent modes in the rigid-lid, inviscid limit. The frequencies of the WISHE Matsuno modes are not greatly modified, though all of the $n = 0$ modes and smaller scale $n = -1$ modes ($k \geq 5$) have slower phase speeds than their rigid-lid counterparts. Comparing with the growth rates in the stratosphere-only case shown in Fig. 5, we can see that the damping effects of the stratosphere and surface friction are approximately additive.

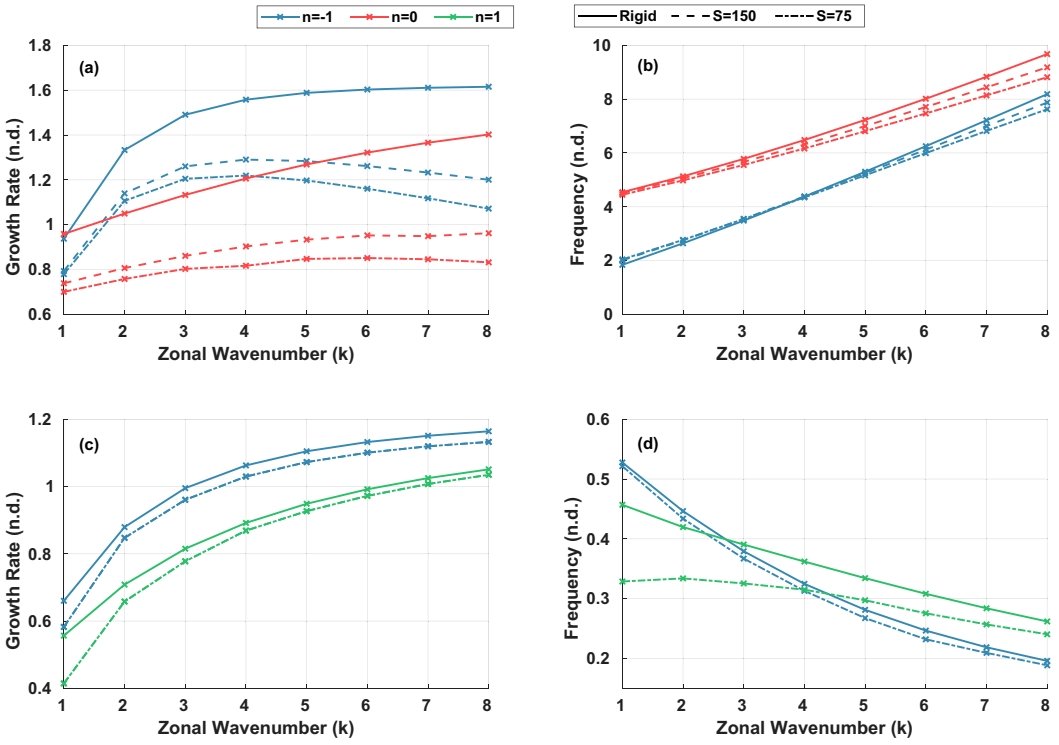

FIG. 10. (a),(c) Non-dimensional growth rate and (b),(d) non-dimensional phase speed for the $n = -1, 0, 1$ modes of the rigid-lid system (solid), the surface friction + rigid-lid system with $S = 150$ and $F = 0.1$ (dashed), and the surface friction + rigid-lid system with $S = 75$ and $F = 0.1$ (dot–dashed). For (a) and (b), the non-dimensional parameters selected are $\alpha = 3.5$, $\chi = 0.5$, $C = 0$, $\gamma = 1$, $D = 2.5$, $G = 0.25$, and $\delta_x = 15$; for (c) and (d), these are $\alpha = 1$, $\chi = 1$, $C = 2.5$, $\gamma = 2$, $D = 1$, $G = 0.02$, and $\delta_x = 30$. Only $S = 75$ case is shown for (c) and (d).

The more interesting question, perhaps, is if the barotropic mode behaves differently when it can be excited by surface friction and also interact with the stratosphere. To examine this, we decompose the horizontal divergence of the barotropic mode into $\partial u/\partial x$, $\partial v/\partial y$, and the sum of both, which is equivalent to the pressure vertical velocity at the tropopause. Figure 11 shows the barotropic mode velocities and the barotropic horizontal divergence decomposition for the $n = 0$, $k = 1$ WISHE Matsuno mode, for a realistic stratosphere stratification ($S = 75$), as well as a highly stratified one ($S = 500$). In the case with a highly stratified stratosphere, we see the long-tail feature of the barotropic mode velocities, as also seen in the surface friction under a rigid-lid model. However, a key differing feature is that the barotropic mode velocities are no longer completely nondivergent, as evidenced in Fig. 11b. Further, the horizontal divergence of the barotropic mode (or, equivalently, the tropopause vertical velocity) decays to zero very quickly poleward, around $|y| = 3$. This is because near the equator, $\partial u_0/\partial x$ and $\partial v_0/\partial y$ have the same sign, evidence that the barotropic mode is exciting the stratosphere near the equator. In contrast, despite the barotropic velocities being small (though nonzero) poleward of the equator, the horizontal divergence is zero because $\partial u_0/\partial x$ and $\partial v_0/\partial y$ have opposite signs and almost exactly cancel. This is evidence of a tropospherically trapped barotropic mode. When we reduce the stratosphere stratification to $S = 75$, as shown in Figs. 11c and 11d, in effect allowing the tropopause to be leakier, we see that the poleward extent of the barotropic mode velocities is greatly reduced, and hence the poleward extent of $\partial u_0/\partial x$ and $\partial v_0/\partial y$ is also reduced. The horizontal divergence still decays to zero around $|y| = 3$, as in the case where $S = 500$.

These numerical experiments illustrate the role the S plays in modulating the poleward extent of the barotropic mode. The mechanism can be reasoned as the following: under infinite stratification, (the rigid lid), surface friction allows for the excitement of the barotropic mode far away from the equator, as shown earlier. As the stratification of the stratosphere is decreased, more wave energy escapes into the stratosphere, reducing the poleward extent of the barotropic mode. Despite the unrealistically large stratification ($S = 500$) used to emphasize the characteristics of the trapped barotropic mode, the qualitative behavior of the model does not change with intermediate stratifications (not shown). In other words, the poleward extent of the tropospherically trapped barotropic mode increases with S.

Figures 10c and 10d show the non-dimensional growth rate and phase speeds for the slow modes, for which we obtain by choosing the same parameter set as used in Fig. 3 and 6. Note, the $n = 0$ waves do not grow in time. The growth rates are not modified greatly from the rigid-lid solutions; surface friction seems to have a weaker damping effect on the slower

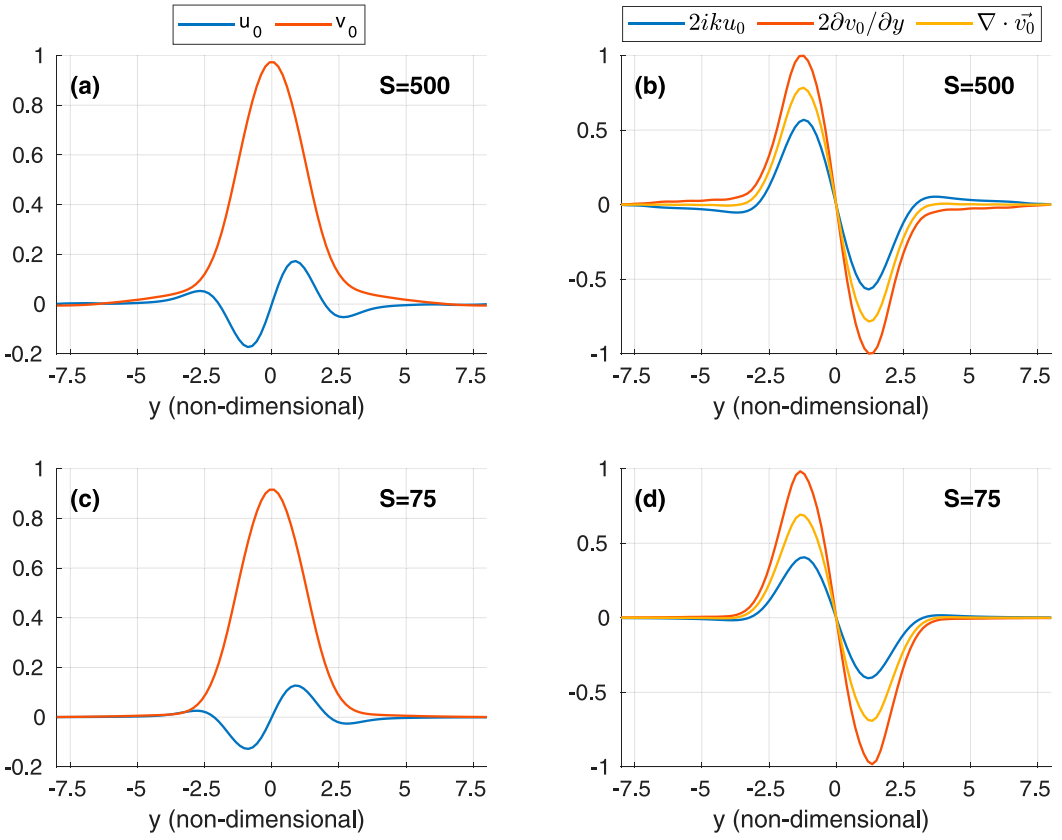

FIG. 11. (a),(c) Barotropic mode zonal and meridional velocities for the WISHE modified Matsuno $n = 0$, $k = 1$ mode using the same parameter set as in Fig. 8, that is, $\alpha = 3.5$, $\chi = 0.5$, $C = 0$, $\gamma = 1$, $D = 2.5$, $G = 0.25$, $\delta_x = 15$, and $F = 0.1$, but with (a) $S = 500$ and (c) $S = 75$. (b),(d) $2(\partial u_0/\partial x)$ and $2(\partial v_0/\partial y)$ (scaled by 2), and $\nabla \cdot \mathbf{v}_0$ for the same mode, but with (b) $S = 500$ and (d) $S = 75$.

propagating modes. The damping effect of the stratosphere on the growth rates is small but the greatest at the largest scales, and almost negligible for the smaller scale waves, as before. However, the frequencies/phase speeds for the slow modes are reduced, by as much as 30% for the $k = 1$ wave. The damping of the frequency is much greater for the $n = 1$ slow propagating modes than the $n = -1$ modes, and much stronger for larger scale $n = 1$ waves. It is also worth noting that the $S = 150$ case is not shown for the slow modes since the lines are nearly indistinguishable from the $S = 75$ case.

The behavior of the poleward extent of the barotropic mode for the slow modes is similar to that for the WISHE-modified Matsuno modes. Figure 12 shows that the barotropic mode associated with the $n = 1$, $k = 2$ slow mode becomes nondivergent away from the equator and trapped in the troposphere. However, one key difference is that the slow modes do not leak much energy into the stratosphere to begin with, and thus decreasing the stratosphere stratification does not completely eliminate the long-tailed behavior of the barotropic velocities. This is evidenced by the small magnitude of the horizontal divergence of the barotropic mode (Figs. 12b,d), regardless of the stratosphere stratification, as iku_0 and $\partial v_0/\partial y$ nearly cancel close to the equator ($|y| < 3$), and exactly cancel for $|y| > 3$.

What are the physical parameters that control the non-dimensional stratosphere stratification, S, and how can they vary across different equatorial waves? The non-dimensionalization of S [see appendix A] suggests that the stratosphere buoyancy frequency N^2 and the meridional length scale L_y are quantities that could potentially lead to large variations in S. The value of L_y depends on a multitude of factors that can vary greatly in the tropics, such as the troposphere dry stratification, moist adiabatic lapse rate, and the precipitation efficiency. The largest influencing factor, however, is the precipitation efficiency ϵ_p: waves with larger ϵ_p experience a much greater stratosphere stratification. For instance, for Earth-like parameters and a $\epsilon_p = 0.5$, $S \approx 20$, while for $\epsilon_p = 0.95$, $S \approx 200$, an order of magnitude difference. While our definition of ϵ_p is an egregiously simple parameterization of cloud microphysics, the impact of ϵ_p on S links cloud microphysical properties to the behavior of the barotropic mode.

4. Discussion and summary

In this study, we extended a previously developed linear framework to include two mechanisms that can excite the barotropic mode in equatorial waves, surface friction, and coupling to the stratosphere. We first analyzed the modification

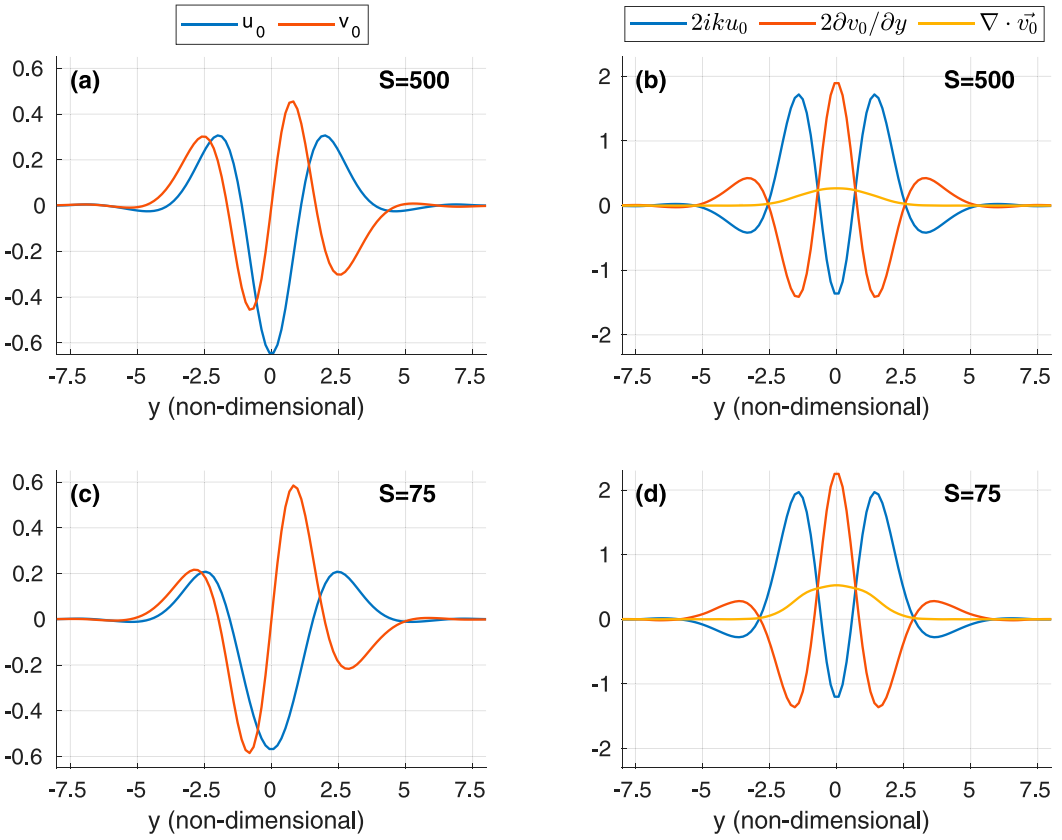

FIG. 12. As in Fig. 11 but for the slow-propagating $n = 1$, $k = 2$ mode using the parameter set $\alpha = 1$, $\chi = 1$, $C = 2.5$, $\gamma = 2$, $D = 1$, $G = 0.02$, $\delta_s = 30$, and $F = 0.1$.

of equatorial waves in the two separate limits of 1) coupling to the stratosphere with an inviscid surface, and 2) surface friction under a rigid lid. Using a combination of theoretical solutions for the $v = 0$ mode and numerical solutions for higher-order meridional modes, we found that the presence of a stratosphere leads to upward wave energy propagation that strongly dampens the growth rate of smaller-scale waves. This effect is consistent across the WISHE-modified Matsuno modes explored in this study, though it does not appreciably affect the slow propagating modes that are destabilized from cloud-radiative feedbacks. The barotropic mode is found to lead the baroclinic mode for the $n = -1$ eastward-propagating modes, leading to a slight eastward tilt in the vertical that arises from the superposition of the two modes. The eastward tilt was found to be robust across horizontal scales and stratosphere stratification. In the limit of surface friction under a rigid lid, we found that surface friction acts only to dampen growth rates by nearly a constant across all waves and zonal wavenumbers, which is reasonable given that surface friction acts on a constant time scale of damping in our framework. We also found that frictional excitation of the barotropic mode leads to long tails of nondivergent barotropic zonal and meridional velocities away from the equator. The barotropic mode is also found to lead the baroclinic mode for the $n = -1$ eastward-propagating modes, leading to a vertical tilt in the zonal wind field, but not the vertical velocity field since the barotropic mode is nondivergent under a rigid lid.

The combined effects of surface friction and coupling to the stratosphere were analyzed using numerical solutions of the full linear model. We found that for the growth rates of the waves, the damping effects of surface friction and coupling to the stratosphere were approximately additive. Under a large non-dimensional stratosphere stratification, both the WISHE-modified Matsuno modes and slow modes exhibit tropospherically trapped barotropic modes away from the equator. Thus, the nondivergent barotropic velocities extend far away from the equator and are small but nonzero. When the non-dimensional stratosphere stratification is reduced, the poleward extent of the barotropic mode is greatly reduced. These results indicate that the dimensional variables that influence the non-dimensional stratosphere stratification, such as the buoyancy frequency in the stratosphere and precipitation efficiency, play key roles in modulating the poleward extent of the barotropic mode. While this study was restricted to theoretical analysis of the barotropic mode, future work will attempt to find evidence of the barotropic mode in both observational and numerical data.

This work models the interaction of equatorial waves with a zero-mean-flow stratosphere, and is the first basic step to illuminate how a dynamically dry and passive fluid influences

the dynamics of a moist and convecting fluid underneath. Extension of the framework developed in this study to a non-zero mean flow in the stratosphere will be the subject of future work, which would allow for an investigation into the extent to which upward wave radiation can explain the observed relationship between the MJO and quasi-biennial oscillation (QBO) (Yoo and Son 2016).

Finally, it is worth discussing some of the shortcomings of the modeling framework. Our application of surface friction in an infinitesimally small boundary layer with zero vertical velocity is exceptionally crude compared to real-world frictional boundary layers. In addition, the strict-quasi equilibrium approximation may not be as accurate for extremely short or high-frequency waves (Ahmed et al. 2021), as evidenced by the presence of what looks like a second baroclinic mode in observations of convectively coupled Kelvin waves (Straub and Kiladis 2002). Regardless, both surface friction and upward radiation of wave energy are shown to important mechanisms that influence the horizontal structure, vertical structure, and growth rates of equatorial waves, through excitation of the barotropic mode.

Acknowledgments. The authors gratefully acknowledge the support of the National Science Foundation through Grant NSF ICER-1854929. The authors thank two anonymous reviewers and Dr. Juliana Dias for their helpful suggestions, which greatly improved the manuscript.

Data availability statement. Model source code, instructions, and code to generate the figures from outputs of the numerical model are available at github.com/linjonathan. All code and figures were generated using MatLab.

APPENDIX A

Model Formulation Details

a. Non-dimensionalization

Here, we define the non-dimensional scalings for the variables that appear in the full linear model. The scalings for the tropospheric quantities $s^{*\prime}$, s'_m, χ, α, γ, D, and G are identical to those described in the appendix of KE18:

$$x \rightarrow ax, \tag{A1}$$

$$y \rightarrow L_y y, \tag{A2}$$

$$p \rightarrow (p_s - p_t)\hat{p}, \tag{A3}$$

$$z^* \rightarrow Hz^*, \tag{A4}$$

$$t \rightarrow \frac{a}{\beta L_y^2} t, \tag{A5}$$

$$L_y^4 \rightarrow \frac{\Gamma_d}{\Gamma_m} \frac{d\overline{s}_d}{dz}(T_b - [\overline{T}])H \frac{1-\epsilon_p}{\beta^2}, \tag{A6}$$

$$u' \rightarrow \frac{aC_k|\overline{\mathbf{V}}|}{H} u', \tag{A7}$$

$$v' \rightarrow \frac{L_y C_k|\overline{\mathbf{V}}|}{H} v', \tag{A8}$$

$$w^{*\prime} \rightarrow C_k|\overline{\mathbf{V}}|w^{*\prime}, \tag{A9}$$

$$\phi' \rightarrow \frac{a\beta L_y^2 C_k|\overline{\mathbf{V}}|}{H} \phi', \tag{A10}$$

$$\omega \rightarrow \frac{C_k\overline{\mathbf{V}}(p_s - p_t)}{H} \omega, \tag{A11}$$

$$N^2 \rightarrow \frac{\beta^2 L_y^4}{H^2} S, \tag{A12}$$

$$F \rightarrow \frac{aC_d|\overline{\mathbf{V}}|}{\beta L_y^2 h_b}, \tag{A13}$$

where most dimensional parameters are described in the main text and in KE18. Parameters not defined in this text are the mean radius of the Earth a, the dry adiabatic lapse rate γ_d, the moist adiabatic lapse rate γ_m, the dry entropy stratification $d\overline{s}_d/dz$, the precipitation efficiency ϵ_p, and the enthalpy exchange coefficient C_k. The terms on the left side of the arrow are the dimensional quantities, and those on the right side are the non-dimensional quantities.

b. Numerical model

The full mathematical description of the numerical system (including damping terms) is below:

$$\frac{\partial u_0}{\partial t} = -ik(\phi_s + V_1(\hat{p}_t)s^*) + yv_0 - 2F(u_0 + u_1) - ru_0, \tag{A14}$$

$$\frac{\partial v_0}{\partial t} = \delta_x\left\{-\frac{\partial}{\partial y}(\phi_s + V_1(\hat{p}_t)s^*) - yu_0\right\} - F(v_0 + v_1) - rv_0, \tag{A15}$$

$$\frac{\partial u_1}{\partial t} = iks^* + yv_1 - 2F(u_0 + u_1) - ru_1, \tag{A16}$$

$$\frac{\partial v_1}{\partial t} = \delta_x\left(\frac{\partial s^*}{\partial y} - yu_1\right) - F(v_0 + v_1) - rv_1, \tag{A17}$$

$$\frac{\partial s^*}{\partial t} = (1 + C)s_m - w - \alpha(u_0 + u_1) - \chi s^* - rs^*, \tag{A18}$$

$$\gamma\frac{\partial s_m}{\partial t} = -Ds^* - \alpha(u_0 + u_1) - Gw + Cs_m - rs_m, \tag{A19}$$

$$w = -ik(u_0 + u_1) - \frac{\partial}{\partial y}(v_0 + v_1), \tag{A20}$$

$$\frac{\partial u_s}{\partial t} = -ik\phi_s + yv_s - ru_s, \tag{A21}$$

$$\frac{\partial v_s}{\partial t} = \delta_x\left(-\frac{\partial \phi_s}{\partial y} - yu_s\right) - rv_s, \tag{A22}$$

$$\frac{\partial \phi_s}{\partial t} = -\int_\infty^z w_s^* S\, dz^* - r\phi_s, \tag{A23}$$

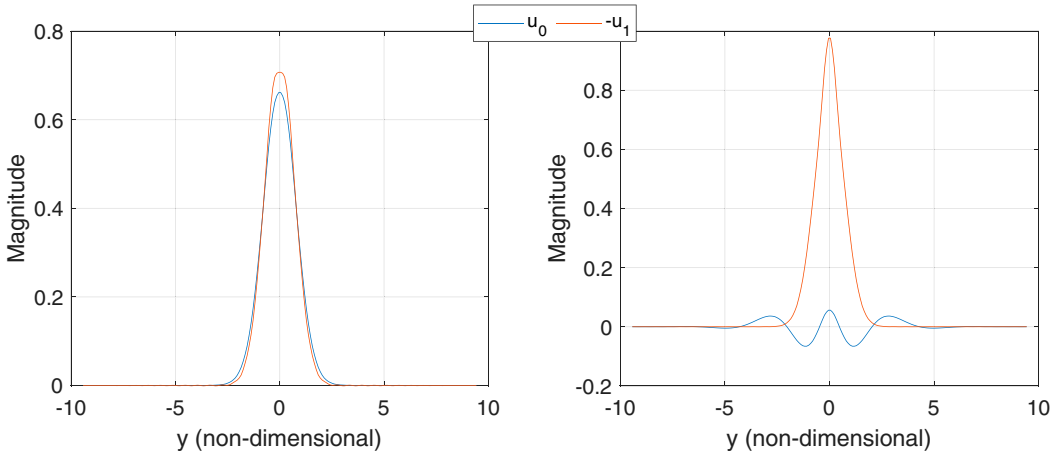

FIG. B1. (left) Barotropic and negative of the baroclinic wind linear response to a $k = 0$, steady forcing in SST $[s^* = \exp(-y^2/2)]$ with no damping, WISHE, or cloud-radiative feedbacks, but nonzero surface friction $F = 0.1$, under a highly stratified stratosphere $S = 150$. A small amount of meridional diffusion ($\eta = 0.01$) is required for numerical stability. (right) As in the left panel, but for the $k = 1$ response to a $k = 1$ forcing.

$$\rho_s w_s^* = -B\left(iku_0 + \frac{\partial v_0}{\partial y}\right) - \int_{z^*=1}^{z}\left\{\rho_s\left(iku_s(y,z^*) + \frac{\partial}{\partial y}v_s(y,z^*)\right)\right\}dz^*, \quad \text{(A24)}$$

where all variables are defined in the main text with the exception of r, which is the sponge coefficient for the sponge layer that is applied at the boundaries of the domain.

The spectral filtering is important to prevent any small scale, undesired noise from dominating the domain, and to ensure the isolation of the mode of interest. The spectral filter $\hat{F}(l)$ is highly selective for only the largest wavenumbers, which contain almost all of the energy for the large-scale modes:

$$F(l)\frac{1}{2}\tanh\left(\left|\frac{l}{2.5}\right| - 9.5\right)\frac{1}{2}. \quad \text{(A25)}$$

where l is the meridional wavenumber. At the end of every time step, the time tendency of each prognostic variable is transformed to Fourier space and multiplied by $\hat{F}(l)$. The time tendency of the prognostic variables is then retransformed back into physical space (y). The constants in the spectral filter were carefully tuned over experimentation.

APPENDIX B

Poleward Extent of Barotropic Mode

To understand the poleward extent of the barotropic mode under the simplest dynamics, we start with the vorticity equation for the barotropic mode under a rigid lid:

$$\sigma\zeta_0 + v_0 = -F\left(\frac{1}{\delta_x}\frac{\partial v_0}{\partial x} - 2\frac{\partial u_0}{\partial y} + \frac{1}{\delta_x}\frac{\partial v_1}{\partial x} - 2\frac{\partial u_1}{\partial y}\right), \quad \text{(B1)}$$

where the barotropic mode vorticity $\hat{\zeta}_0 = \hat{\nabla}_H \times \mathbf{v}_0$ and $\hat{\nabla}_H = [(1/\delta_x)\partial/\partial x, \partial/\partial y]$. Considering only steady, zonally symmetric solutions for large δ_x (approximate zonal geostrophy), we have

$$v_0 - 2F\frac{\partial u_0}{\partial y} = 2F\frac{\partial u_1}{\partial y}. \quad \text{(B2)}$$

Under a rigid lid, the barotropic mode must be nondivergent. Thus, zonally symmetric circulations must have $\partial v_0/\partial y = 0$, or $v_0 = 0$ under zero boundary conditions. Zonally symmetric, rigid-lid circulations, then, must have

$$u_0 = -u_1$$

(note that based on the non-dimensionalization, this is equivalent to zero total wind at the surface, but nonzero winds at the tropopause). This means that the poleward extent of the barotropic mode is the same as that of the baroclinic mode. Figure B1 (left) shows an experiment calculating the steady linear response to a steady, exponentially decaying forcing in sea surface temperature $[s^* = \exp(-y^2/2)]$, with no damping, WISHE, or cloud-radiative feedbacks, but nonzero surface friction $F = 0.1$, under a highly stratified stratosphere $S = 150$. A small amount of meridional diffusion ($\eta = 0.01$) is required for numerical stability. Besides the small effects of diffusion, the baroclinic and barotropic zonal winds are nearly overlapping.

For non-zonally symmetric circulations, like the waves considered in the paper, the situation becomes very different. This is because v_0 is no longer zero, since it is only the horizontal divergence of the barotropic mode that must be zero. When zonal barotropic winds are excited through surface friction, v_0 must be comparable in magnitude (at least for large-scales, for instance, $k = 1$). What is the behavior of u_0 in this case? In Eq. (B2), we eliminate v_0 in favor of u_0 by using the fact that the horizontal divergence of the barotropic mode is zero under rigid lids:

$$iku_0 + 2F\frac{\partial^2 u_0}{\partial y^2} = -2F\frac{\partial^2 u_1}{\partial y^2}. \quad \text{(B3)}$$

Equation (B3) is of parabolic form. If one considers the steady problem with forcing in the baroclinic mode (such as, from an SST forcing), then the response in the barotropic mode will have a larger meridional extent than the source term. Figure B1, right, shows the steady linear response of the zonal winds, but now to a $k = 1$ SST forcing. Now, the barotropic winds have a much larger meridional extent, as observed in the equatorial waves.

The form of u_1 can be easily deduced from an SST forcing, when considering the meridional baroclinic momentum equation, under steady solutions:

$$0 = \delta\left(\frac{\partial s}{\partial y} - yu_1\right) - F(v_0 + v_1).$$

For $\delta \gg F$, the zonal baroclinic winds are nearly in geostrophic balance. In other words, surface friction does not significantly modify the baroclinic circulation. Mathematically, this is

$$\frac{\partial s}{\partial y} = yu_1.$$

For our exponentially decaying SST anomaly centered on the equator, $s(y) = \exp(-y^2/2)$, the baroclinic zonal winds are: $u_1(y) = -\exp(y^2/2)$.

REFERENCES

Adames, Á. F., and J. M. Wallace, 2014: Three-dimensional structure and evolution of the vertical velocity and divergence fields in the MJO. *J. Atmos. Sci.*, **71**, 4661–4681, https://doi.org/10.1175/JAS-D-14-0091.1.

——, and D. Kim, 2016: The MJO as a dispersive, convectively coupled moisture wave: Theory and observations. *J. Atmos. Sci.*, **73**, 913–941, https://doi.org/10.1175/JAS-D-15-0170.1.

Ahmed, F., J. D. Neelin, and Á. F. Adames, 2021: Quasi-equilibrium and weak temperature gradient balances in an equatorial beta-plane model. *J. Atmos. Sci.*, **78**, 209–227, https://doi.org/10.1175/JAS-D-20-0184.1.

Andrews, D. G., J. R. Holton, and C. B. Leovy, 1987: *Middle Atmosphere Dynamics*. Vol. 40, Academic Press, 489 pp.

Arakawa, A., and W. H. Schubert, 1974: Interaction of a cumulus cloud ensemble with the large-scale environment, Part I. *J. Atmos. Sci.*, **31**, 674–701, https://doi.org/10.1175/1520-0469(1974)031<0674:IOACCE>2.0.CO;2.

Betts, A. K., 1982: Saturation point analysis of moist convective overturning. *J. Atmos. Sci.*, **39**, 1484–1505, https://doi.org/10.1175/1520-0469(1982)039<1484:SPAOMC>2.0.CO;2.

Chao, W. C., and B. Chen, 2001: The role of surface friction in tropical intraseasonal oscillation. *Mon. Wea. Rev.*, **129**, 896–904, https://doi.org/10.1175/1520-0493(2001)129<0896:TROSFI>2.0.CO;2.

Chumakova, L. G., R. R. Rosales, and E. G. Tabak, 2013: Leaky rigid lid: New dissipative modes in the troposphere. *J. Atmos. Sci.*, **70**, 3119–3127, https://doi.org/10.1175/JAS-D-12-065.1.

Edman, J. P., and D. M. Romps, 2017: Beyond the rigid lid: Baroclinic modes in a structured atmosphere. *J. Atmos. Sci.*, **74**, 3551–3566, https://doi.org/10.1175/JAS-D-17-0140.1.

Emanuel, K. A., 1987: An air-sea interaction model of intraseasonal oscillations in the tropics. *J. Atmos. Sci.*, **44**, 2324–2340, https://doi.org/10.1175/1520-0469(1987)044<2324:AASIMO>2.0.CO;2.

——, 2020: Slow modes of the equatorial waveguide. *J. Atmos. Sci.*, **77**, 1575–1582, https://doi.org/10.1175/JAS-D-19-0281.1.

——, J. D. Neelin, and C. S. Bretherton, 1994: On large-scale circulations in convecting atmospheres. *Quart. J. Roy. Meteor. Soc.*, **120**, 1111–1143, https://doi.org/10.1002/qj.49712051902.

Gill, A. E., 1980: Some simple solutions for heat-induced tropical circulation. *Quart. J. Roy. Meteor. Soc.*, **106**, 447–462, https://doi.org/10.1002/qj.49710644905.

Horel, J. D., and J. M. Wallace, 1981: Planetary-scale atmospheric phenomena associated with the Southern Oscillation. *Mon. Wea. Rev.*, **109**, 813–829, https://doi.org/10.1175/1520-0493(1981)109<0813:PSAPAW>2.0.CO;2.

Hsu, P., and T. Li, 2012: Role of the boundary layer moisture asymmetry in causing the eastward propagation of the Madden–Julian oscillation. *J. Climate*, **25**, 4914–4931, https://doi.org/10.1175/JCLI-D-11-00310.1.

Khairoutdinov, M. F., and K. Emanuel, 2018: Intraseasonal variability in a cloud-permitting near-global equatorial aquaplanet model. *J. Atmos. Sci.*, **75**, 4337–4355, https://doi.org/10.1175/JAS-D-18-0152.1.

Kiladis, G. N., K. H. Straub, and P. T. Haertel, 2005: Zonal and vertical structure of the Madden–Julian oscillation. *J. Atmos. Sci.*, **62**, 2790–2809, https://doi.org/10.1175/JAS3520.1.

Kuang, Z., 2008a: Modeling the interaction between cumulus convection and linear gravity waves using a limited-domain cloud system–resolving model. *J. Atmos. Sci.*, **65**, 576–591, https://doi.org/10.1175/2007JAS2399.1.

——, 2008b: A moisture-stratiform instability for convectively coupled waves. *J. Atmos. Sci.*, **65**, 834–854, https://doi.org/10.1175/2007JAS2444.1.

Mapes, B. E., 2000: Convective inhibition, subgrid-scale triggering energy, and stratiform instability in a toy tropical wave model. *J. Atmos. Sci.*, **57**, 1515–1535, https://doi.org/10.1175/1520-0469(2000)057<1515:CISSTE>2.0.CO;2.

——, and R. A. Houze, 1995: Diabatic divergence profiles in western Pacific mesoscale convective systems. *J. Atmos. Sci.*, **52**, 1807–1828, https://doi.org/10.1175/1520-0469(1995)052<1807:DDPIWP>2.0.CO;2.

Matsuno, T., 1966: Quasi-geostrophic motions in the equatorial area. *J. Meteor. Soc. Japan*, **44**, 25–43, https://doi.org/10.2151/jmsj1965.44.1_25.

Moskowitz, B. M., and C. S. Bretherton, 2000: An analysis of frictional feedback on a moist equatorial Kelvin mode. *J. Atmos. Sci.*, **57**, 2188–2206, https://doi.org/10.1175/1520-0469(2000)057<2188:AAOFFO>2.0.CO;2.

Neelin, J. D., and I. M. Held, 1987: Modeling tropical convergence based on the moist static energy budget. *Mon. Wea. Rev.*, **115**, 3–12, https://doi.org/10.1175/1520-0493(1987)115<0003:MTCBOT>2.0.CO;2.

——, and J.-Y. Yu, 1994: Modes of tropical variability under convective adjustment and the Madden–Julian Oscillation. Part I: Analytical theory. *J. Atmos. Sci.*, **51**, 1876–1894, https://doi.org/10.1175/1520-0469(1994)051<1876:MOTVUC>2.0.CO;2.

——, and N. Zeng, 2000: A quasi-equilibrium tropical circulation model—Formulation. *J. Atmos. Sci.*, **57**, 1741–1766, https://

doi.org/10.1175/1520-0469(2000)057<1741:AQETCM>2.0.CO;2.

Raymond, D. J., and Ž. Fuchs, 2007: Convectively coupled gravity and moisture modes in a simple atmospheric model. *Tellus*, **59A**, 627–640, https://doi.org/10.1111/j.1600-0870.2007.00268.x.

Sobel, A. H., and C. S. Bretherton, 2000: Modeling tropical precipitation in a single column. *J. Climate*, **13**, 4378–4392, https://doi.org/10.1175/1520-0442(2000)013<4378:MTPIAS>2.0.CO;2.

——, and E. Maloney, 2013: Moisture modes and the eastward propagation of the MJO. *J. Atmos. Sci.*, **70**, 187–192, https://doi.org/10.1175/JAS-D-12-0189.1.

——, J. Nilsson, and L. M. Polvani, 2001: The weak temperature gradient approximation and balanced tropical moisture waves. *J. Atmos. Sci.*, **58**, 3650–3665, https://doi.org/10.1175/1520-0469(2001)058<3650:TWTGAA>2.0.CO;2.

Straub, K. H., and G. N. Kiladis, 2002: Observations of a convectively coupled Kelvin wave in the eastern Pacific ITCZ. *J. Atmos. Sci.*, **59**, 30–53, https://doi.org/10.1175/1520-0469(2002)059<0030:OOACCK>2.0.CO;2.

Vallis, G. K., 2017: *Atmospheric and Oceanic Fluid Dynamics*. Cambridge University Press, 745 pp.

Wang, B., 1988: Dynamics of tropical low-frequency waves: An analysis of the moist Kelvin wave. *J. Atmos. Sci.*, **45**, 2051–2065, https://doi.org/10.1175/1520-0469(1988)045<2051:DOTLFW>2.0.CO;2.

——, and H. Rui, 1990: Dynamics of the coupled moist Kelvin–Rossby wave on an equatorial β-plane. *J. Atmos. Sci.*, **47**, 397–413, https://doi.org/10.1175/1520-0469(1990)047<0397:DOTCMK>2.0.CO;2.

Wheeler, M., and G. N. Kiladis, 1999: Convectively coupled equatorial waves: Analysis of clouds and temperature in the wavenumber–frequency domain. *J. Atmos. Sci.*, **56**, 374–399, https://doi.org/10.1175/1520-0469(1999)056<0374:CCEWAO>2.0.CO;2.

Xu, K., and K. A. Emanuel, 1989: Is the tropical atmosphere conditionally unstable? *Mon. Wea. Rev.*, **117**, 1471–1479, https://doi.org/10.1175/1520-0493(1989)117<1471:ITTACU>2.0.CO;2.

Yano, J.-I., and K. Emanuel, 1991: An improved model of the equatorial troposphere and its coupling with the stratosphere. *J. Atmos. Sci.*, **48**, 377–389, https://doi.org/10.1175/1520-0469(1991)048<0377:AIMOTE>2.0.CO;2.

Yoo, C., and S.-W. Son, 2016: Modulation of the boreal wintertime Madden–Julian Oscillation by the stratospheric quasi-biennial oscillation. *Geophys. Res. Lett.*, **43**, 1392–1398, https://doi.org/10.1002/2016GL067762.